PROF. JOSEPH R. MOSKAL (Orcid ID : 0000-0002-4813-3297)

Article type : Original Article

Title: NYX-2925 induces metabotropic NMDAR signaling that enhances synaptic NMDAR and AMPAR

Running head: NYX-2925 increases synaptic GluN2B and AMPAR

M. Scott Bowers[1,2,*], Luisa P. Cacheaux[2], Srishti U. Sahu[1], Mary E. Schmidt[2], Joseph A. Sennello[2], Katherine Leaderbrand[2], M. Amin Khan[2], Roger A. Kroes[1,2], Joseph R. Moskal[1,2]

[1.] Falk Center for Molecular Therapeutics, Biomedical Engineering, Northwestern University, Evanston, IL 60201, USA;
[2.] Aptinyx, Inc., Evanston, IL 60201, USA

[*]**Corresponding Author**:
M. Scott Bowers, PhD
Aptinyx, Inc.
Falk Center for Molecular Therapeutics
Biomedical Engineering
Northwestern University
1801 Maple Ave, Suite 4300
Evanston, IL 60201

Phone: 847-871-0377
Email: scottbowers@aptinyx.com

Cover art description:
N-methyl-D-aspartate receptors (NMDARs) mediate a number of physiological and pathophysiological processes. We sought to determine if the novel NMDAR modulator NYX-2925, discovered by Aptinyx Inc. and currently in Phase 2 clinical development for chronic pain conditions, increases glutamatergic neurotransmission. The rat primary hippocampal neuron depicted on the cover was treated with NYX-2925 at concentrations that increase synaptic levels of GluN2B-containing NMDARs via a novel ion-flux independent mechanism, which in turn, increases the ability of chemical long-term potentiation to increase synaptic levels of GluA1-containing α-amino-3-hydroxy-5-methyl-4-isoxazolepropionic acid (AMPA) receptors. Green: PSD-95 positive puncta, Red: GluA1 positive puncta, Blue: MAP-2 positive puncta

Abstract

N-Methyl-D-Aspartate receptors (NMDARs) mediate both physiological and pathophysiological processes, *though selective* ligands lack broad clinical utility. NMDARs are composed of multiple subunits, but GluN2 is predominately responsible for functional heterogeneity. *Specifically*, the GluN2A- and GluN2B-containing subtypes are enriched in adult hippocampus and cortex and impact neuronal communication via dynamic trafficking into and out of the synapse. We sought to understand if NYX-2925, a novel NMDAR modulator, alters synaptic levels of GluN2A- or GluN2B-containing NMDARs. Low-picomolar NYX-2925 increased GluN2B colocalization with the excitatory post-synaptic marker PSD-95 in rat primary hippocampal neurons *within 30 min. Twenty-four hours* following oral administration, *1 mg/kg* NYX-2925 increased GluN2B in PSD-95-associated complexes *ex vivo*, and *low-picomolar NYX-2925* regulated numerous trafficking pathways *in vitro*. Because the NYX-2925 concentration that *increases* synaptic GluN2B was markedly below that which enhances long-term potentiation *(mid-nanomolar)*, we sought to elucidate the basis of this effect. Although NMDAR-dependent, NYX-2925-mediated colocalization of GluN2B with PSD-95 occurred independent of ion flux, as colocalization increased in the presence of either the NMDAR channel blocker MK-801 or glycine site antagonist 7CK. *Moreover*, *while mid-nanomolar* NYX-2925 concentrations, which do not increase synaptic GluN2B, enhanced calcium transients, *functional plasticity was only* enhanced by picomolar NYX-2925. Thus, NYX-2925 concentrations that increase synaptic GluN2B facilitated the chemical long-term potentiation (chemLTP) induced insertion of synaptic α-amino-3-hydroxy-5-methyl-4-isoxazolepropionic acid receptor GluA1 subunit levels. Basal (unstimulated by chemLTP) levels of synaptic GluA1 were *only increased* by *mid-nanomolar* NYX-2925. These data suggest that NYX-2925 facilitates homeostatic plasticity by initially increasing synaptic GluN2B via metabotropic-like NMDAR signaling.

Keywords: NMDA, AMPA, trafficking, colocalization, metabotropic, LTP (**6/6 words**)

Abbreviations

AAALAC: Association for Assessment and Accreditation of Laboratory Animal Care

aCSF: artificial cerebrospinal fluid

AMPAR: α-amino-3-hydroxy-5-methyl-4-isoxazolepropionic acid receptor

APV: D-(-)-2-amino-5-phosphonovaleric acid

chemLTP: chemical long-term potentiation

7CK: 7-chlorokynurenic acid

DIV: days in vitro

EC_{50}: concentration at which 50% of the population is activated

FWHM: full width at half maximum

GluA1: -amino-3-hydroxy-5-methyl-4-isoxazolepropionic acid receptor subunit 1

GluN1: N-methyl-D-aspartate receptor subunit 1

GluN2A: N-methyl-D-aspartate receptor subunit 2, subtype A

GluN2B: N-methyl-D-aspartate receptor subunit 2, subtype B

LTP: long-term potentiation

LTD: long-term depression

MK-801**:** (5R,10S)-(**–**)-5-Methyl-10,11-dihydro-5H-dibenzo[a,d]cyclohepten-5,10-imine hydrogen maleate

MS: mass spectral

NBQX: 2,3-Dioxo-6-nitro-1,2,3,4-tetrahydrobenzo[f]quinoxaline-7-sulfonamide disodium salt

NMDAR: N-methyl-D-aspartate receptor

NYX-2925: ((2S, 3R)-3-hydroxy-2-((R)-5-isobutyryl-1-oxo-2,5-diazaspiro[3,4]octan-2-yl) butanamide

PO: per os (by mouth; oral administration)

PSD-95: post-synaptic density protein 95

RRID: Research Resource Identifier

TTX: tetrodotoxin

1. Introduction

N-methyl-D-aspartate receptors (NMDARs) are ligand-gated cation channels thought to play critical roles in brain plasticity and higher cognitive functions (Bliss and Collingridge, 1993). NMDAR dysfunction is associated with psychiatric and neurological disorders including depression, neuropathic pain, PTSD, and age-related cognitive decline, among others (Kumar, 2015; Aiyer et al., 2017; Ghasemi et al., 2017; Krystal et al. 2017). However, currently available NMDAR ligands exhibit low clinical utility (Chen and Lipton, 2006). Accordingly, there is much interest in developing novel NMDAR modulators with therapeutic potential.

The NMDAR is a heterotetrameric complex composed of multiple subunits; the specific combination of these subunits imparts unique biophysical, pharmacological, and signaling properties to channel function (Vicini et al., 1998; Cull-Candy and Leszkiewicz, 2004; Traynelis et al., 2010; Paoletti, 2011). Briefly, all NMDARs contain two obligatory GluN1 subunits and two additional subunits that can be comprised of GluN2 (A through D subtypes) and/or GluN3 (A or B subtype), but the GluN2 subunit is thought to be the major determinant of NMDAR functional heterogeneity (Monyer et al., 1992; Ishii et al., 1993; Monyer et al., 1994; Vicini et al., 1998; Cull-Candy and Leszkiewicz, 2004; Gielen et al., 2009; Yuan et al., 2009; Traynelis et al., 2010; Paoletti, 2011).

In the adult hippocampus and cortex, GluN2A and GluN2B are the predominantly expressed GluN2 subunits (Monyer et al., 1994), and NMDARs containing these GluN2 subtypes are heterogeneously partitioned between synaptic, perisynaptic, and extrasynaptic membranes. This partitioning suggests that specific NMDAR composition uniquely impacts neuronal integration of synaptic and extrasynaptic inputs (Groc et al., 2009). Previous work has found that the GluN2A and GluN2B subtypes are dynamically trafficked into and out of the synaptic membrane by NMDAR agonists (Barria and Malinow, 2002) and co-agonists (Nong et al., 2003; Ferreira et al., 2017). Thus, NMDARs (particularly those containing the GluN2B subtype) are highly mobile and can exchange

between synaptic and extrasynaptic sites (Tovar and Westbrook, 2002; Groc et al., 2006; Ferreira et al., 2017).

Here, we sought to understand if the NMDAR modulator, NYX-2925, regulates synaptic levels of GluN2A and GluN2B. NYX-2925 is an orally bioavailable non-peptide mimetic of GLYX-13, which is also known as Rapastinel. In rat models, both NYX-2925 (Khan et al., 2017) and GLYX-13 (Moskal et al., 2017) are cognitive enhancers that facilitate synaptic plasticity. In brief, we found that NYX-2925 exhibits a unique biphasic dose response. Mid-nanomolar concentrations mediate calcium transients and long-term potentiation (LTP) (Khan et al., 2017), whereas picomolar concentrations engage hippocampal homeostatic plasticity by augmenting synaptic levels of GluN2B via a metabotropic-like mechanism of the NMDAR. Next, we found that NYX-2925 pretreatment enhanced activity-dependent synaptic insertion of α-amino-3-hydroxy-5-methyl-4-isoxazolepropionic acid receptors (AMPARs). Given the NYX-2925 dose-response profile and increasing appreciation of non-ionotropic modes of NMDAR signal transduction (Dore et al., 2017), this study demonstrates that NYX-2925 is a powerful tool to probe both canonical and novel modes of NMDAR signaling.

2. Methods

2.1 Reagents

All reagents were obtained in the highest quality possible from standard vendors. NYX-2925 [((2S, 3R)-3-hydroxy-2-((R)-5-isobutyryl-1-oxo-2,5-diazaspiro[3.4]octan-2-yl) butanamide] was synthesized by Sai Life Sciences (Telangana, IND). D-(-)-2-amino-5-phosphonovaleric acid (APV; *PubChem ID: 135342*), 7-chlorokynurenic acid (7CK; *PubChem ID: 1884*), (5R,10S)-(–)-5-Methyl-10,11-dihydro-5H-dibenzo[a,d]cyclohepten-5,10-imine hydrogen maleate (MK-801; *PubChem ID: 6420042*), tetrodotoxin (TTX; *PubChem ID: 16759596*), strychnine *(PubChem ID: 16219987)*, and bicuculline *(PubChem ID: 6852386)* were obtained from Tocris (Minneapolis, MN, USA). 2,3-Dioxo-6-nitro-

1,2,3,4-tetrahydrobenzo[f]quinoxaline-7-sulfonamide disodium salt (NBQX; *PubChem ID: 3272523*) and nimodipine *(PubChem ID: 4497)*, and NMDA *(Cat #: ab120052)* were obtained from Abcam (Cambridge, MA, USA). Unless otherwise noted, cell culture reagents were obtained from Fisher (Gibco, Waltham, MA, USA; *RRID: SCR_008452*).

2.2 Animal housing and treatment

Animal use was approved by the Northwestern University Institutional Animal Care and Use Committee (OLAW assurance: D16-00182 (A3283-01) expiration 5/31/22; AAALAC accreditation 10/9/85). After delivery, timed dams (Envigo, Indianapolis, IN, USA) were allowed to acclimate in an AAALAC-accredited vivarium for at least 24 h before embryos were harvested. Food and water were provided *ad libitum* and lights were on a 12 h cycle (lights on 06:00). For in vivo studies, P60 male Sprague Dawley rats (Envigo) were housed 3 per cage for 1 wk in the vivarium prior to experimentation. Next, rats *(n = 3 animals per treatment group; no animals were excluded)* received vehicle (1 mL/kg, 0.5% carboxy methyl cellulose in water, P.O.) or NYX-2925 (1 mg/kg, 0.5% carboxymethylcellulose in water, P.O.). *Animals were not anesthetized during drug treatment.* Twenty-four h after treatment, the prefrontal cortex was isolated on ice and snap frozen. All animals were euthanized by rapid decapitation. *Power analysis was not performed, no data were excluded (no exclusion criteria were pre-determined), and no animals died during experimentation.*

2.3 Primary culture

Primary hippocampal cultures were prepared as previously described (Nault and De Koninck, 2010). Briefly, hippocampi were extracted from embryonic day 18 Sprague Dawley rat pups *(Charles River Laboratories, MA, USA; RRID:RGD_737891) and brains from a given litter pooled and* placed into cold Hibernate E. Tissue was washed and chopped with a scalpel prior to enzymatic digestion (10 min, Papain, BrainBits, Springfield, Il, USA) at 37˚C and subsequent washing with plating media (MEM *Cat #: 11090081*, supplemented with 10% fetal bovine serum *Cat #: 26400044* from Hyclone, Logan, UT, USA; 2 mM Glutamax® *Cat #: 35050061*; 1 mM sodium pyruvate *Cat #: 111360070*; and

10 μg /mL penicillin/ 10 μg/mL streptomycin *Cat #: 15-140-122*). Next, cells were triturated with a polished pipette, strained (100 μm), and dropped onto 12 mm glass poly-D-lysine coverslips (neuVitro, Vancouver, WA, USA, *Cat #: CC-12-pdl*) at $3.5x10^5$ cells per mL. After 90 min, cells were flooded with un-supplemented Neurobasal® *(Cat #: 21-103-049)* and plating media applied. Four hours later, 50% of the media was exchanged with Neurobasal® that was supplemented with B27, Glutamax®, and penicillin/streptomycin. Three days later, cells were treated with 3 μM cytosine arabinoside (AraC; Sigma-Aldrich, St. Louis, MO, USA, *Cat #: C1768)*) for 24 h and 50% of the media was replaced with fresh, supplemented Neurobasal®. Thereafter, cells were fed twice per week by exchanging 50% of the media with supplemented Neurobasal® until cultures were used at 14-15 days *in vitro*.

2.4 NYX-2925 treatment

All solutions were prepared and brought to 37˚C on the day of the experiment. Treatment groups consisted of coverslips (prepared as described above) from multiple plates, and all experiments were run in at least duplicate from *independent cell culture preparations*. Cells were washed with artificial cerebrospinal fluid (aCSF; in mM: 119 NaCl, 30 glucose; 10 HEPES; 5 KCl; 2 $CaCl_2$, 2 $MgCl_2$, pH 7.4) and allowed to recover in aCSF at 37˚C for 30 min. Next, vehicle or glutamate (final concentration 50 μM) and/or NYX-2925 *(0.1 pM – 30 nM)* were co-applied for 30 or 60 min. The rationale for quantifying drug effect at these time points was based upon the findings that NYX-2925 facilitated LTP when bath applied to rat hippocampal slices for 40 min and that the maximum concentration of NYX-2925 in the rat cerebral spinal fluid occurs 60 min after oral dosing (Khan et al., 2018). Cells were washed (cold PBS) and then processed for immunocytochemistry, harvested in RIPA with protease and phosphatase inhibitors (1:100, Sigma-Aldrich, St. Louis, MO). Blockers of the NMDAR glutamate site (APV), glycine site (7CK), or channel (MK-801) were included in both the recovery and drug-treatment buffer, when indicted below. Because MK-801 is an activity-dependent channel blocker, MK-801 was both pre-incubated (30 min) and co-applied with NYX-2925.

Application of MK-801 in this manner blocks any NMDARs that may be activated by ligand or spontaneous activity of primary hippocampal cultures (Siebler et al., 1993). 7CK was similarly used with both a pre-incubation and co-application.

2.5 Immunocytochemistry of GluN2-containing NMDARs and PSD-95

After washing with cold PBS, cells were fixed on ice with cold 4% p-formaldehyde (EMS, Hatfield, PA, USA, *Cat #: 50-980-487*) in 4% sucrose/PBS for 7 min. After washing, cells were blocked in 1% normal goat serum (MP Biomedicals, Santa Ana, CA, USA, *Cat #: ICN642921*) at 4˚C and then incubated with mouse primary antisera directed against the extracellular domain of GluN2A (1:800, Biolegend, San Diego, CA, USA; *RRID: AB_2564953*) or GluN2B (1:1,000, Biolegend; *RRID: AB_2564823*). After washing, secondary antibody incubation (1:200, goat anti-mouse AF594, Probes, Waltham, MA, USA, *RRID: AB_2534091*), subsequent wash, and post-fix (2% p-formaldehyde, 5 min, 4˚C), cells were permeabilized (0.25% Triton X-100® *Cat #: BP151*), and intracellular epitopes blocked (1% normal goat serum). Next, endogenous biotin was blocked (Vector Labs, Burlingame, CA, USA, *Cat #: NC9406552*) prior to incubation with mouse biotinylated primary directed against PSD-95 (1:1,000, SYSY, Goettingen, DEU; *RRID: AB_10804286*) and chicken primary directed against microtubule associated protein 2 (MAP2; 1:5,000, Abcam, Cambridge, MA, USA; RRID: *AB_2138153*). Primary antisera were detected with NeutrAvidin Dylight® 488 (1:200, Fisher Scientific, Waltham, MA, USA; *Cat #: PI22832*) or goat anti-chicken AF647 (1:3,000, Probes, Waltham, MA, USA; *RRID: AB_2535866*) prior to mounting in Prolong Gold (Probes). Antisera were centrifuged (10,000 x g, 5 min, 4˚C) immediately prior to use.

2.6 Immunoblotting

Neurons were collected in RIPA buffer with protease inhibitors (1:100, Fisher; *Cat #: 78444*), sonicated, and centrifuged (20 min, 14,000xg, 4˚C). Protein in supernatant was quantified (Pierce 660 nm assay, Thermo Scientific, Waltham, MA, USA; Cat #: PI22663). Thirty-five micrograms of

protein were run on a 4 - 20% gradient polyacrylamide gel and transferred onto a 0.22 μm nitrocellulose membrane. Blots were blocked in 5% non-fat dry milk (Bio-Rad, Hercules, CA, USA, *Cat #: 1706404*) and incubated with primary antibody as follows: GluN2A (1:1,000, Cell Signaling, overnight, 4°C, *RRID: AB_2112295*), GluN2B (1:1,000, Cell Signaling, overnight, 4°C, *RRID: AB-1264223*), PSD-95 (1:5,000, Millipore, Burlington, MA, overnight, 4°C, *RRID: AB_10807979*) or β-actin HRP (1:5,000, Cell Signaling, 1 h, room temperature, *RRID: AB_1903890*), followed by host-specific secondary antibody for 1 h at room temperature (1:2,000 of goat anti-rabbit HRP (Cell Signaling, *RRID: AB_2099233*) or goat anti-mouse Alexa Fluor® 647 (Probes, Waltham, MA, USA, *RRID: AB_2535804*). Blots were imaged (Bio-Rad Chemidoc, Hercules, CA, USA) and band intensity was analyzed using Image Lab 6.0.1 (Bio-Rad).

2.7 Proteomic analysis of rat hippocampal cultures

Sample preparation. Hippocampal cultures, prepared as above, were treated with either 1 pM or 30 nM NYX-2925 for 30 minutes, also as described above (n = 4 *independent cell culture preparations*). Treated cultures were washed in cold PBS and frozen at -80°C until analysis. Subsequent sample handling, mass spectrometry, and data analysis were performed by MSBioworks LLC (Ann Arbor, MI, USA). Cells were lysed in 500 μL urea buffer (8 μM urea, 50 mM Tris HCl, 150 mM NaCl, 1X Roche [Indianapolis, IN, USA] Complete Proteinase Inhibitor [Sigma-Aldrich St. Louis, MO, *Cat #: 11836145001*, pH 8.0). Samples were incubated at room temperature for 1 h, clarified by centrifugation, and quantified by Qubit fluorometry (Life Technologies). A 50 μg aliquot of each sample was digested in solution using the following protocol: sample was diluted in 25 mM ammonium bicarbonate *(Cat #: A643)*, reduced with 10 mM dithiothreitol *(Cat #: AAJ1539706)* at 60°C, alkylated using 50 mM iodoacetamide *(Cat #: AC122270050)* at room temperature, digested with 2.5 μg trypsin (Promega, Madison, WI, USA, *Cat #: V5280*) at 37°C for 18 h followed by quenching with formic acid. Peptides were cleaned using solid phase extraction using the Empore C18 plate (3M, St. Paul, MN, USA, *Cat #: 14-378-57*).

Mass Spectrometry. Peptides (2 µg per sample) were analyzed by nano LC/MS/MS with a NanoAcquity HPLC system (Waters) interfaced to a Fusion Lumos mass spectrometer (Thermo Fisher). Peptides were loaded on a trapping column and eluted over a 75 µm analytical column at 350 nL/min; both columns were packed with Luna C18 resin (Phenomenex, Torrance, CA, USA, *Cat #: 00G-4252-E0*). Each sample was separated over a 4 h gradient. The mass spectrometer was operated in data-dependent mode, with MS and MS/MS performed in the Orbitrap at 60,000 FWHM resolution and 15,000 FWHM resolution, respectively. The instrument was run with a 3 s cycle for MS and MS/MS.

Data Processing. Data were processed through the MaxQuant software v1.6.0.16 (www.maxquant.org), normalized using the LFQ algorithm, peptide IDs searched using Andromeda (Cox et al., 2011) with peptide and protein FDR < 0.01, and analyzed using Perseus v1.5.5.3 (http://www.coxdocs.org). Statistically significant differences in protein content between drug-treated and vehicle groups were assessed by Student's t-Test. The level of statistical significance was set at $p < 0.05$.

Ontological Analyses. Ingenuity® Pathway Analysis (IPA®; Qiagen Germantown, MD, USA) was used to identify overrepresented canonical pathways associated with significantly differentially expressed proteins ($p < 0.05$) identified in the proteomic data sets. The IPA algorithm interrogates a published, curated database of protein interrelationships (Krämer et al., 2014) to identify coordinated regulation of biological pathways associated with drug treatment. Multiple hypothesis correction based on the Benjamini–Hochberg approach at 1% FDR threshold was implemented. Statistical significance of pathway enrichment was determined by Fisher's exact test ($p < 0.05$).

2.8 Proteomic analysis of rat prefrontal cortex PSD-95 co-immunoprecipitates

PSD-95 co-immunoprecipitation. Tissues from rat prefrontal cortex *(n = 3 per treatment group)* isolated 24 hr following drug treatment were lysed by sonication in RIPA buffer with protease inhibitors (1:100, Sigma, St. Louis, MO, USA). Following centrifugation (10 min, 14,000 x g, 4˚C), protein in supernatant was quantified (BCA, Thermo Scientific, Waltham, MA, USA). Ten micrograms of PSD-95 antibody (Millipore, Burlington, MA, USA) was incubated with 6 mg of magnetic beads (Dynabeads Protein G, Thermo Scientific, Burlington, MA, USA, 2 h, 4˚C) and crosslinked (5 mM bis-sulfosuccinicimidyl suberate (BS3), Thermo Fisher, Burlington, MA, USA) for 30 minutes prior to quenching (1 M Tris-HCl, pH 7.5,15 min) and overnight incubation with 1 mg of rat prefrontal cortex protein. Antibody-bound protein was eluted by boiling beads (100˚C, 5 min), and eluent was analyzed by mass-spectrometry.

MS Sample Preparation. Each sample was separated on a 10% Bis-Tris Novex® mini-gel (Life Technologies) using the 2-(N-morpholino)ethanesulfonic acid (MES) buffer system. The gel was stained with Coomassie and each lane excised into ten equally sized segments. Gel pieces were robotically processed (ProGest, DigiLab) with the following protocol: (a) washed with 25 mM ammonium bicarbonate followed by acetonitrile, (b) reduced with 10 mM dithiothreitol at 60°C followed by alkylation with 50 mM iodoacetamide at RT, (c) digested with trypsin (Promega, Madison, WI, USA) at 37°C for 4 h and quenched with formic acid. The supernatant was analyzed directly without further processing.

Mass Spectrometry. Each gel digest was analyzed by nano LC/MS/MS with a NanoAcquity® HPLC system (Waters, Milford, MA, USA) interfaced to a Q Exactive® (Thermo Fisher). Peptides were loaded on a trapping column and eluted over a 75 µm analytical column at 350 nL/min; both columns were packed with Jupiter Proteo® resin (Phenomenex, Torrance, CA, USA). The mass spectrometer was operated in data-dependent mode, with MS and MS/MS performed in the

Orbitrap (Thermo Fisher) at 70,000 FWHM and 17,500 FWHM resolution, respectively. The fifteen most abundant ions were selected for MS/MS.

Data Processing. Data were searched using Mascot (Matrix Scientific, Boston, MA, USA) using 10 ppm peptide mass tolerance, 0.02 Da fragment mass tolerance with a maximum of 2 missed cleavages. Mascot DAT files were parsed into Scaffold (Proteome Software, Portland, OR, USA) for validation, filtering, and to create a non-redundant list per sample. Data were filtered at 1% protein and peptide level false discovery rate (FDR) requiring at least two unique peptides per protein.

2.9 Calcium transients

Calcium imaging was performed on primary *hippocampal (or cortical for Supplementary material)* neurons at DIV 20 - 22. Cells were loaded with 2 µM Fluo-4-AM (Thermo Fisher, *Cat #: F14202*) dissolved in pluronic F-127 (*Cat #: P3000MP*) and 20% anhydrous DMSO (Molecular Probes, *Cat # D12345*) for 20 minutes at room temperature in buffer (in mM: 145 NaCl, 5.4 KCl, 1.8 $CaCl_2$, 11 glucose, 10 HEPES, pH 7.4). For dye loading, 50 µM APV was also added to the buffer. After dye loading, cells were washed three times with buffer containing APV and left at room temperature for 15 minutes before imaging to complete deesterification of the dye. The cells were then washed with extracellular buffer without APV and transferred to a microscope chamber. Extracellular buffer containing 500 nM TTX, *10 µM NBQX (2 µM for cortical cultures), and 10 µM nimodipine (0 M for cortical)* was perfused onto the cells for 3 - 4 min to wash off the APV. Fluo-4-AM fluorescence in the cells was detected with an Eclipse Ti2 fluorescent microscope (Nikon), SOLA SE II 365 Light Engine (Lumencor, Beaverton, OR, USA), and DS-Fi3 camera (Nikon) at 20x magnification. The experiments were performed at room temperature, and images were acquired at 1 frame/2 s. After acquisition of a 1.5 min baseline, 4 µM NMDA was washed onto the cells for 1 min followed by a 2 min washout. NYX-2925 (either 1 pM or 30 nM) plus 4 µM NMDA was then washed onto the cells for 1 min followed by a 2 min washout. 10 µM NMDA plus 3 µM D-serine was washed onto the cells at

the end to elicit a "max" response. For data analysis, relative fluorescence intensity ($\Delta F/F_0$) was calculated. The maximum $\Delta F/F_0$ values for the initial NMDA response as well as for NYX-2925 + NMDA were used to calculate % enhancement values. Cells whose initial NMDA response was larger than 40% of the "max" response were excluded.

2.10 Chemical induction of LTP (chemLTP)

ChemLTP was conducted as previously described (Lu et al., 2001). Following vehicle or NYX-2925 treatment (30 min), cells were washed and placed into chemLTP buffer (in mM: 140 NaCl, 33 glucose, 25 HEPES, and 2 $CaCl_2$; in M: 200 glycine, 25 bicuculline, 1 TTX, and 1 strychnine) for 3 min at 37˚C prior to being placed in recovery buffer for 20 min (in mM: 140 NaCl, 33 glucose, 25 HEPES, and 2 $CaCl_2$; in μM: 25 bicuculline, 1 TTX, and 1 strychnine) at 37˚C. The chemLTP vehicle cohort was placed into recovery buffer twice instead of chemLTP buffer followed by recovery buffer. Next, cells were washed (cold PBS) and fixed on ice (4% p-formaldehyde, 4% sucrose, in PBS) for 13 min prior to blocking (10% donkey serum, Sigma-Aldrich, St. Louis, MO, USA *Cat #: D9663*) and incubation with rabbit primary antisera for GluA1 (1:10, 1 h, 4˚C, Millipore, *RRID: AB-564636*) as described (Ohashi et al., 2016), and cy3-labelled secondary (Jackson ImmunoResearch, West Grove, PA, USA *RRID: AB_2307443*). Immunocytochemistry for PSD-95 and MAP2 proceeded as described above.

2.11 Confocal microscopy and image analysis

Images were acquired with a Yokogawa CSU-X1 spinning disk (Tokyo, JPN) by a blinded experimenter. All images were taken with a Plan Apo 60X oil objective (1.42 numerical aperture) mounted on a Ti2 confocal microscope (Nikon, Tokyo, JPN) equipped with an FRAPPA camera (Andor, Belfast, UK) and NIS-Elements AR 4.51.01 (Nikon, Tokyo, JPN). Image stacks were acquired at Nyquist (generally 50 – 60 individual planes), each 512 x 512 pixels in size (12 bit). Refractive index was 1.515 and pinhole was 45.98 μm. Channel acquisition order was far-red, red, green, and then blue. Laser power, exposure time, and averaging were optimized to avoid saturation and parameters

were held constant across experiments. No more than 4 images were acquired from a single coverslip across 4 coverslips in at least duplicate *from independent cell culture preparations*. Images were processed by NIS Elements (Nikon) and analyzed with Volocity 6.1.1 (Quorum, Puslinch, Ontario, CAN). A 1.5 lower limit standard deviation threshold was applied to images, and based upon ultrastructural measurements of the post-synaptic density (Sheng and Hoogenraad, 2007), immunolabeled puncta were identified GluN2-containing NMDAR and GluA1-containing AMPARs (AMPAR: 10 μM radius, 1 μM^3 minimum object size; PSD-95: 10 μM radius, 0.5 μM^3 minimum object size). Colocalization was measured as the mean intensity of GluN2 subtypes or GluA1 subunit puncta within PSD-95 puncta. A field of view contributed one n to the analysis. Thus, mean colocalization of 14 – 28 cells (in at least biological duplicate) were analyzed per treatment.

2.12 Statistical analysis

Outliers were determined as lying greater than two standard deviations from the mean for each treatment group. Exclusions include Figure 1f (n = 1 from 1 nM), Figure 3a (n = 2 from pM, n = 1 pM + MK801), Figure 3c (n = 1 from 1 nM. After determining normal distribution of the data (K-S Normality Test), data were analyzed by one-way ANOVA or paired Student's t-Test, as indicated, at 95% confidence (Statview *5.0,* Berkeley, CA, USA). Where appropriate, significant main effects were investigated by *post-hoc* analysis, *as indicated in the figure legends*. All data are presented as mean ± the standard error of the mean (SEM) *with whiskers indicating data spread*.

3. Results

3.1 NYX-2925 increases synaptic GluN2B in vitro.

Rat primary hippocampal neurons were cultured for 14 days prior to bath application of NYX-2925 with or without 50 μM glutamate for 30 or 60 min. (**Figure 1a**). Dose selection was based on the previous finding that picomolar NYX-2925 in the presence of 50 μM glutamate selectively

potentiates [^{3}H]MK-801 binding to GluN2B-containing receptors, whereas nanomolar NYX-2925 does so in all GluN2 subtypes, including GluN2A (Khan et al., 2018). Following treatment, cells were washed, fixed, and immunolabeled for surface GluN2A or GluN2B and intracellular PSD-95 to determine the effects of NYX-2925 treatment on synaptic localization of GluN2-containing NMDARs. Representative immunolabeling and specific fluorophore detection of GluN2A, GluN2B, and PSD-95 is indicated (**Figure 1b - d**). NMDAR colocalization with PSD-95 is used as a proxy for synaptically localized receptor because it is generally thought that the NMDAR is retained in the synaptic membrane via binding of the C-terminal domain to PDZ domain-containing proteins, including PSD-95 (Prybylowski et al., 2005; Al-Hallaq et al., 2007; Bard et al., 2010).

Using this approach, the effect of NYX-2925 on synaptic GluN2A and GluN2B levels was studied. Application of NYX-2925 (0.1 pM – 30 nM) in the presence of glutamate for 30 min did not increase colocalization of GluN2A with PSD-95 in primary neurons (**Figure 2a**). Next, an expanded dose-response curve was conducted for the GluN2B subtype. After 30 min, synaptic GluN2B increased only at low picomolar NYX-2925 concentrations in the presence of glutamate ($F(9,130) = 7.019$, $p = 0.0001$, n = 14 cells per group; **Figure 2b**). The increase in colocalization seen after NYX-2925 treatment is NMDAR-dependent because colocalization did not increase in the presence of the NMDAR glutamate site antagonist APV (compared to vehicle, $p > 0.05$; compared to NYX-2925, $p < 0.05$; **Figure 2b**). Moreover, *post-hoc* analysis showed that neither 1 picomolar NYX-2925 nor glutamate alone were sufficient to increase synaptic GluN2B (both compared to vehicle, $p > 0.05$; **Figure 2b**). Whole-cell protein content of GluN2A, GluN2B, and PSD-95 *were decreased by glutamate, but not further* altered by either 1 picomolar *or 30 nanomolar NYX-2925 (**Figure 2c - e**; GluN2A: $F(3,26) = 1.46$, $p < 0.0001$; GluN2B: $F(3,26) = 0.94$, $p < 0.0001$; PSD-95: $F(3,26) = 34.52$, $p < 0.001$).* The *increase in* synaptic GluN2B levels mediated by low picomolar NYX-2925 appears to be transient *in vitro*, as colocalization returned to baseline after continuous drug treatment *at the same concentration* for 60 min ($F(1,26) = 1.01$, $p = 0.32$, n = 14 cells per group; **Figure 2f**). *Continuous*

exposure to higher NYX-2925 concentrations (30 nM) for 60 min significantly reduced colocalization of GluN2B with PSD-95 (F3,52) = 5.66, p = 0.002, n = 14 cells per group; ***Figure 2f****). In contrast to the transient effects induced by continuous exposure to low NYX-2925 concentrations, increased GluN2B levels were seen in PSD-95 coimmunoprecipitates of the rat prefrontal cortex 24 h after dosing (1 mg/kg, p.o.; Supplementary Material; the relationship of this dose with the concentrations studied in vitro is discussed below).* Lastly, representative immunolabeling is indicated (**Figure 2g**). Together, these data indicate that *picomolar concentrations of* NYX-2925 function with glutamate via the NMDAR to increase synaptic localization of GluN2B.

3.3 NYX-2925 increases synaptic GluN2B independent of ion flux through NMDARs.

Given that nanomolar NYX-2925 concentrations facilitate synaptic plasticity *ex vivo* (Khan et al., 2018), it is intriguing that picomolar, but not nanomolar concentrations increased synaptic GluN2B. Accordingly, we sought to better understand how NYX-2925 acts on GluN2B-containing NMDARs. As before, primary *hippocampal* neurons were co-treated with 1 picomolar NYX-2925 and 50 μM glutamate for 30 min, and colocalization of GluN2B with PSD-95 was measured. A one-way ANOVA found a main effect of treatment ($F(13,238) = 7.72$, $p = 0.0001$, n = 14 – 28 cells), and *post-hoc* analysis showed increased colocalization ($p < 0.05$) that was blocked by APV (compared to vehicle, $p > 0.05$; compared to NYX-2925 + glutamate, $p < 0.05$; **Figure 3a**). However, the NYX-2925-mediated increase in colocalization was not prevented by either the NMDAR channel blocker MK-801 (compared to vehicle, $p < 0.05$; compared to NYX-2925 + glutamate; $p > 0.05$) or the glycine site antagonist 7CK (compared to vehicle, $p < 0.05$; compared to NYX-2925 + glutamate, $p > 0.05$; **Figure 3a**). *Post-hoc* analysis also revealed that colocalization of GluN2B-containing NMDARs with PSD-95 was unaffected by treatment with other combinations of these ligands (compared to vehicle, $p > 0.05$; **Figure 3a**). These data suggest that picomolar NYX-2925 recruits synaptic GluN2B-containing NMDARs via a metabotropic-like mechanism of the NMDAR. Representative immunolabeling is indicated (**Figure 3b**).

In order to verify that 1 picomolar NYX-2925 did not affect calcium transients following activation of NMDARs, calcium imaging was performed using rat primary *hippocampal* neurons. A low concentration of NMDA (4 µM) was washed onto the cells followed by washout to establish a baseline response for each cell. NYX-2925 in the presence of 4 µM NMDA was then washed onto the cells to determine if NYX-2925 enhanced calcium transients beyond NMDA alone. *Neither* the 1 picomolar *nor 1 nanomolar* concentration of NYX-2925 enhanced calcium flux, whereas 30 nanomolar NYX-2925 resulted in a *15.2% enhancement (t(5)=4.608, p = 0.011*; **Figure 3c**). *A similar dose-related effect of NYX-2925 in mediating calcium transients was also observed in primary cortical neurons (**Figure S1;** 11.5% enhancement at 30 nM, but not 1 pM).*

3.4 NYX-2925 activates trafficking pathways in vitro.

Next, we sought to determine whether the rapid, differential effects on GluN2 trafficking observed in primary hippocampal cultures following NYX-2925 treatment were associated with alterations in global proteome dynamics. Thus, we coupled comprehensive proteomics with ontological bioinformatics analysis. A total of 4,860 unique rat proteins (as annotated by ~33,000 unique peptides) were detected across all samples at a false discovery rate of 0.01. When comparing cells treated with 1 pM NYX-2925 for 30 minutes with vehicle-treated cells, 196 significantly differentially expressed ($p < 0.05$) proteins were identified: 122 proteins were up-regulated and 74 were down-regulated. When comparing cells treated with 30 nM NYX-2925 for 30 minutes with vehicle-treated cells, 338 significantly differentially expressed ($p < 0.05$) proteins were identified: 261 proteins were up-regulated and 77 were down-regulated.

Subsequent ontological analysis revealed that the dose-dependent proteomic profiles were remarkably distinct in terms of the pathways directly relevant to both receptor trafficking and synaptic plasticity. **Tables 1** and **2** summarize these findings, and expanded proteomic results are located in **Supplementary Tables 1** and **2**. Exposure of cultures to a metabotropic-like dose of NYX-

2925 (1 pM) resulted in significant modulation of pathways associated with NMDAR trafficking, and included marked inhibition of clathrin-mediated endocytosis, ($p < 3.5 \times 10^{-04}$), EIF2 (9.33×10^{-10}), and mTOR (2.24×10^{-8}) signaling as well as an increase in the protein kinase A pathway ($p < 1.86 \times 10^{-04}$); such modulation could result in increased number and stabilization of membrane receptors.

Conversely, exposure to an ionotropic dose of NYX-2925 (30 nM) significantly up-regulated proteins comprising pathways associated with synaptic LTP ($p < 2.69 \times 10^{-8}$) as well as pathways associated with receptor expression and trafficking, including EIF2 ($p < 1.00 \times 10^{-4}$), CDK5 ($p < 1.00 \times 10^{-4}$), 14-3-3 ($p < 1.28 \times 10^{-4}$), and protein kinase A ($p < 1.86 \times 10^{-6}$); these signaling pathways are associated with synaptic targeting, clustering, and recycling of receptors into and out of the synapse (**Table 2**).

3.5 NYX-2925 facilitates the chemLTP-mediated increase in synaptic GluA1.

Next, we sought to understand the functional impact NYX-2925 has on neuronal communication. Because frequency-dependent forms of *inducing* LTP affect a localized synaptic area, we *instead* studied a chemical form of LTP (chemLTP), which can stimulate the entire culture (Ahmad et al., 2012). *The primary readouts of the* chemLTP protocol that we used (high glycine, no magnesium) are increased insertion and dendritic clustering of GluA1-containing AMPARs in addition to more frequent miniature excitatory postsynaptic potentials (Lu et al., 2001). *Here,* synaptic levels of GluA1-containing AMPARs were studied because they are responsible for the early phase of LTP (Shi et al., 2001; Romberg et al., 2009), and LTP is absent in GluA1-null mice (Zamanillo et al., 1999). As before, primary hippocampal neurons were treated with vehicle, 1 picomolar, *or 30 nanomolar* NYX-2925 in the presence of 50 μM glutamate (**Figure 4a**). After removing drug, *a subset of* cells from each treatment condition continued through the chemLTP protocol (**Figure 4a**). Representative immunolabeling of GluA1 and PSD-95 is shown (**Figure 4b - d**).

A one-way ANOVA followed by post-hoc analysis found a main effect of NYX-2925 treatment on GluA1 colocalization with PSD-95 in the absence of chemLTP (trafficking-only conditions; F(2,39) =4.64, p = 0.018, n = 14 cells per group ***Figure 4e****). Further, post-hoc analysis found a significant effect at 30 nanomolar (p = 0.0345), but not 1 picomolar (p = 0.5104) NYX-2925. Following chemLTP, a one-way ANOVA showed a main effect of chemLTP on GluA1 colocalization with PSD-95 (F(3,52) = 7.09, p = 0.0004, n = 14 cells per group). Post-hoc analysis revealed that this colocalization was increased similarly by pretreatment with either vehicle (compared to vehicle without chemLTP, p = 0.0259) or 30 nanomolar NYX-2925 (compared to vehicle without chemLTP, p = 0.0313;* ***Figure 4f****). In contrast, even greater GluA1 colocalization with PSD-95 was observed after chemLTP when cells were pretreated with 1 picomolar NYX-2925 (increased colocalization above that caused by either chemLTP alone, p = 0.0243, or 30 nanomolar NYX-2925 followed by chemLTP, p = 0.0201;* ***Figure 4f****). Thus, NYX-2925 concentrations that promote GluN2B colocalization with PSD-95 were found to also facilitate GluA1 colocalization with PSD-95 after chemLTP over levels seen with chemLTP alone. In summary, increased NMDAR stimulation, such as that mediated by either high, ionotropic NYX-2925 concentrations or chemLTP conditions increase synaptic GluA1. In contrast,* low NYX-2925 concentrations *that increase synaptic GluN2B* do not alter synaptic GluA1 levels *on their own, but pre-treatment with this same low, metabotropic-like NYX-2925 concentration* facilitates the chemLTP-mediated recruitment of GluA1 into the synapse. *Thus, the NYX-2925-mediated recruitment of synaptic GluN2B appears to augment synaptic GluA1 insertion following LTP stimulation.* These data agree with prior reports showing that changes in the number or function of NMDARs modulate the LTP induction threshold (Pérez-Otaño and Ehlers, 2005; Abraham, 2008).

4. Discussion

Here, we report that synaptic levels of GluN2B are increased by picomolar concentrations of the recently developed NMDAR modulator NYX-2925 *in vitro*, and this effect was replicated *in vivo*. Thus, NYX-2925 could profoundly impact neuronal communication by facilitating the integration of multiple synaptic inputs via increased GluN2B-mediated calcium transients and/or receptor number (Scimemi et al., 2004). NMDAR activation is required for the NYX-2925-mediated colocalization of GluN2B with PSD-95, as this effect was blocked by the glutamate site antagonist APV. Intriguingly, picomolar NYX-2925 appears to modulate synaptic GluN2B levels independent of NMDAR ion flux, as the resulting colocalization of GluN2B with PSD-95 was unaffected by either a NMDAR channel blocker or glycine site antagonist. This antagonist strategy has been used by others to demonstrate ion flux-independent functions of NMDARs (Nabavi et al., 2013; Dore et al., 2015). Moreover, picomolar NYX-2925 had no effect on NMDA-induced calcium transients in primary neurons. In contrast, nanomolar NYX-2925 concentrations increased calcium transients, but did not affect colocalization of GluN2B with PSD-95 *unless continuously present in the bath for an extended period (60 min)*. These concentration-dependent actions of NYX-2925 were echoed in the divergent signaling pathways activated at either ionotropic or metabotropic-like drug concentrations. Lastly, the functional consequence of NYX-2925 treatment was analyzed via quantification of NMDAR-mediated insertion of the AMPAR subunit GluA1 into the synapse, which was induced with chemLTP. Because picomolar NYX-2925 was found to facilitate chemLTP-induced synaptic GluA1 levels without altering basal GluA1, NYX-2925 may engage this form of homeostatic plasticity via initially recruiting synaptic GluN2B-containing NMDARs through a metabotropic-like mechanism of the NMDAR.

The finding that the NYX-2925-mediated increase in synaptic GluN2B was blocked by APV clearly demonstrates that NYX-2925 operates through NMDARs to exert this effect. Moreover, the observation that neither the channel blocker MK-801 nor the glycine site antagonist 7CK blocked the

NYX-2925-mediated increase in synaptic GluN2B supports the idea that NYX-2925 can act through a metabotropic-like (ion flux-independent) mechanism. The inability of MK-801 and 7CK to prevent long-term depression (LTD) was previously used to support the conclusion that NMDAR-mediated LTD (Nabavi et al., 2013) and signal transduction across the membrane (Dore et al., 2015) can also occur independent of NMDAR ion flux. An additional study found that these antagonists converted the response to a normally ion-flux-dependent, LTP-inducing stimulus into an LTD-like response (Stein et al., 2015). Together with this literature, our findings support the conclusion that NYX-2925 may modulate synaptic NMDAR levels via metabotropic-like signaling of the NMDAR. As reviewed by Dore and colleagues (Dore et al., 2017), the existence and biological relevance of metabotropic NMDAR signaling is an active area of research with several investigators finding both supportive (Yang et al., 2004; Kessels et al., 2013; Nabavi et al., 2013; Tamburri et al., 2013; Dore et al., 2015; Kim et al., 2015; Stein et al., 2015) and contradictory (Babiec et al., 2014; Volianskis et al., 2015; Sanderson et al., 2016) evidence. Among the former, several studies have revealed ion flux-independent trafficking of GluN2-containing NMDARs both by NMDAR agonists (Vissel et al., 2001; Barria and Malinow, 2002) and by co-agonists (Nong et al., 2003; Ferreira et al., 2017). Together, these data add to the rich repertoire by which neuronal communication can be shaped by a growing number of NMDAR modulatory mechanisms.

The findings with low picomolar doses of NYX-2925 reported here add to the growing appreciation that the NMDAR adopts biologically relevant conformational changes independent of channel opening. Other biologically active and therapeutically valuable molecules also function in the low picomolar range. For example, the hepatitis C antiviral pibrentasvir (Mavyret®) exhibits a low picomolar EC_{50}, and was FDA-approved in 2017 for patients with mild cirrhosis and moderate-to-severe kidney disease (Ng et al., 2017). Moreover, both neuropeptide S (Raiteri et al., 2009) and melatonin (Dubocovich, 1983) exert their effects at low picomolar concentrations to modulate neurotransmitter levels.

It is intriguing that pre-incubation of primary hippocampal neurons with picomolar concentrations of NYX-2925 increased the capacity of the neuron to recruit GluA1-containing AMPARs to the synapse following chemLTP. Because picomolar NYX-2925 did not alter colocalization of GluA1 with PSD-95 before chemLTP, such low NYX-2925 concentrations may alter the set-point for LTP induction by increasing synaptic GluN2B levels. Thus, the rapid acting *(within 30 min)* and long-lasting effects of NYX-2925 *(as evident in co-immunoprecipitates taken 24 hrs after treatment in vivo) may* have relevance to homeostatic plasticity processes that are involved in the maintenance and normalization of synaptic function; namely, synaptic scaling and metaplasticity (Abraham and Bear, 1996; Pérez-Otaño and Ehlers, 2005). Homeostatic plasticity regulates the magnitude or direction of activity-dependent plasticity to maintain synaptic scaling within a working range that is typically away from saturation and toxicity. Analogous to the *in vivo* effects observed following administration of NYX-2925, the enhancement of synaptic scaling mediated by low picomolar concentrations *in vitro* occurs primarily through mobilization of both NMDARs and AMPARs into the synapse. Thus, NYX-2925 is a novel tool to control the amount of GluN2B, and upon stimulation, GluA1 in the synapse.

Taken together, our data suggest that NYX-2925 exhibits two dose-dependent mechanisms of action (**Figure 5**). After drug administration, mid-nanomolar NYX-2925 concentrations *likely* mediate traditional NMDAR functions including ion flux and LTP (Khan et al., 2018). NMDARs play critical roles in enduring forms of synaptic plasticity, such as LTP and LTD, and these processes are thought to be a molecular correlate of higher cognitive functions (Bliss and Collingridge, 1993). We previously found that NYX-2925 facilitates LTP at Schaffer collateral-CA1 synapses when applied to hippocampal slices at 500 nM or following oral administration of a dose (1 mg/kg) that yields 44 nM in the cerebral spinal fluid (Khan et al., 2018). *This concentration, as noted above, is near the concentration where we observed facilitated calcium transients (**Figure 3**), and chemLTP-like effects*

*on synaptic localization of GluA1 (**Figure 4**).* This same dose also facilitated novel object recognition and positive emotional learning (Khan et al., 2018) as well as reduced neuropathic pain in rats (Ghoreishi-Haack et al, 2018). Thus, mid-nanomolar NYX-2925 concentrations facilitate cognition and LTP. As concentrations fall *into the low-picomolar range (> 8 h post-oral dosing)*, NYX-2925 *may have* a second, ion flux-independent mechanism of action that engages homeostatic plasticity by lowering the threshold of LTP induction by future stimulation *(**Figure 4**)*. This NYX-2925-mediated homeostatic plasticity is the conceptual counterpoint of a recent report showing that suppressed AMPAR exocytosis contributes to LTD (Fujii et al., 2018). *The ability of NYX-2925 to mediate* homeostatic plasticity is further supported by our prior work showing that NYX-2925 induced metaplasticity ex vivo in rats *24 h after oral dosing* (Khan et al., 2018), *a time at which drug concentrations have passed through the range at which metabotropic-like signaling occurs in vitro (**Figure 3**). Altogether, these data suggest that NYX-2925 may exhibit therapeutic utility by facilitating future plasticity (**Figure 4** and Khan et al. 2018) via increasing synaptic GluN2B as shown both in vitro (**Figure 2**) and in vivo (Khan et al., 2018, Ghoreishi-Haack et al., 2018, and **Supplementary Material**). This pharmacokinetic-based plasticity model (**Figure 5**) should be further validated in future work by determining the effect of specific pharmacokinetic phases (e.g., accumulation, distribution, and elimination) on synaptic GluN2B levels and subsequent chemLTP induction thresholds. Nonetheless, the dose-dependent model of NYX-2925 action is strongly* supported by earlier work showing that lateral diffusion of GluN2B into the synapse engages homeostatic plasticity in intact brain preparations (Zhao et al., 2008).

Although the population of neuronal GluN2A and GluN2B was initially thought to be enriched in the synaptic or extrasynaptic membrane, respectively (Kew et al., 1998; Tovar and Westbrook, 1999; Liu et al., 2004), substantial amounts of extrasynaptic GluN2A and synaptic GluN2B have been identified (Luo et al., 1997; Groc et al., 2006; Thomas et al., 2006; Harris and Pettit, 2007; Petralia et al., 2010), and the relative mobility of these receptor populations are

subtype specific, with GluN2B being more mobile than GluN2A (Groc et al., 2006; Ferreira et al., 2017), and GluN2A less rapidly endocytosed than GluN2B (Lavezzari et al., 2004). Thus, synaptic receptor levels are in a state of dynamic equilibrium being routed into and out of the synapse. While it is currently unknown whether NYX-2925 impacts NMDAR insertion, internalization, or lateralization (Roche et al., 2001; Lavezzari et al., 2003; Lavezzari et al., 2004; Groc et al., 2006), our proteomic studies, conducted at a time point when the effect on trafficking is maximal, revealed that metabotropic-like NYX-2925 concentrations appear to selectively inhibit clathrin-mediated endocytosis while facilitating signaling through protein kinase A. Thus, NYX-2925 appears to increase synaptic GluN2B levels by impairing endocytosis and/or increasing synaptic NMDAR targeting (Crump et al., 2001). *A recent review elegantly highlighted several signaling mechanisms engaged by ion flux-independent activity of the NMDAR (Montes de Oca Balderas, 2018); a number of these were identified in our proteomic analysis following treatment with 1 picomolar NYX-2925.*

In stark contrast to the broad inhibition of signaling mediated by picomolar NYX-2925 (**Table 1**), nanomolar NYX-2925 enhanced a number of unique signaling pathways, the most significant of which was long-term potentiation (**Table 2**). These data also reinforce that NMDAR-mediated calcium influx leads to a multiplicity of effects on receptor-mediated signaling that can modulate receptor trafficking in complex and unpredictable ways. For example, it is well known that the NMDAR is stabilized in the post-synaptic membrane via interaction with several scaffolding proteins collectively known as membrane associated guanylate kinases (MAGUKs) (Wenthold et al., 2003; Elias and Nicoll, 2007). Specifically, the MAGUKs PSD-95 and SAP102 differentially regulate NMDAR trafficking and localization in a GluN2 subtype-specific manner (van Zundert et al., 2004). While MAGUKs play important roles in anchoring NMDARs in the post-synaptic density, deletion of these domains does not ablate functional receptor in the synapse. Additional cellular components that also likely modulate receptor trafficking, synaptic retention, and synaptic remodeling were also represented in this dataset. For example, NMDAR scaffolding can also occur via EphrinB, which can

increase synaptic retention of GluN2A- and GluN2B-containing NMDARs by extracellular domain interactions (Dalva et al., 2000). Additionally, the distinct C-terminal tails of GluN2A and GluN2B subtypes differentially couple to signaling pathways that can regulate receptor trafficking (Lau and Zukin, 2007), dendritic spine remodeling, and synaptic plasticity (Barria and Malinow, 2005; Lisman et al., 2012). For example, phosphorylation of NMDAR by protein kinase C increases both surface NMDAR levels (Lan et al., 2001) and dispersal throughout the dendritic arbor (Fong et al., 2002; Groc et al., 2004).

NMDAR phosphorylation by the sarcoma (Src) family of protein tyrosine kinases, including Fyn kinase, are also known to modulate NMDAR trafficking both by impairing clathrin-dependent endocytosis and via enhancing forward GluN2B trafficking (Levezzari et al., 2003, Trepanier et al., 2012). *Interestingly, Src also appears to regulate PSD-95 multimerization and subsequent clustering of NDMARs within the synapse via cyclin-dependent kinase (CDK5) (Morabito et al., 2004). More specifically, inhibition of CDK5 has been shown to increase Src binding to PSD-95 and subsequent GluN2B phosphorylation of Y1472, which ultimately decreases GluN2B endocytosis (Zhang et al. 2008). Thus, our observation that mid-nanomolar NYX-2925 concentrations do not increase synaptic GluN2B could be due to CDK5 pathway activation, which under these conditions is hypothesized to promote endocytosis. This mechanism may also underlie the decrease in synaptic GluN2B observed here after prolonged exposure (60 min) to 30 nanomolar NYX-2925 as well as the decreased immunocontent in whole cell lysates.*

Src-regulated NMDAR trafficking is also modulated by the small GTPase H-Ras (Thorton et al., 2003). NMDAR trafficking via molecular motors (Yunfei et al., 2015) and/or small GTPases such as Rho, via Citron, (Furuyashiki et al., 1999, Zhang et al. 1999) utilize the actin cytoskeleton. Moreover, proteins comprising the phosphoserine/threonine adaptor protein 14-3-3 pathway have been demonstrated to promote forward trafficking of GluN2-containing NMDARs (Chung et al., 2015). *14-*

3-3 has been shown to bind the actin cytoskeleton in complex with myosin and calmodulin (Münnich et al., 2014). Thus, reorganization of the actin cytoskeleton plays important roles in receptor trafficking during bidirectional synaptic plasticity, including LTP (Kneussel et al. 2013 Okamoto et al., 2004, Petralia et al. 2009). Taken together, our proteomic data underscore that NYX-2925 may modulate synaptic GluN2B levels by engaging several unique biochemical pathways.

Lastly, although the magnitude of changes in synaptic GluN2B reported here might be considered modest, both the magnitude and time course of changes in synaptic NMDAR are consistent with the body of literature. Using electrophysiological and imaging approaches, the maximal NMDAR exchange between the synaptic and extrasynaptic membrane is about 30% (Tovar and Westbrook, 1999; Groc et al., 2004; Groc et al., 2006). Moreover, these and other studies have shown that NMDARs diffuse laterally across the neuronal surface between synaptic and extrasynaptic membranes within a few minutes (Tovar and Westbrook, 1999; Groc et al., 2004; Groc and Choquet, 2006; Groc et al., 2006). The trafficking of distinct GluN2 subtypes into and out of the synaptic membrane is a form of synaptic plasticity that has been associated with a variety of neuropsychiatric and neurological disorders (Pérez-Otaño and Ehlers, 2005; Gardoni et al., 2006; Lau and Zukin, 2007).

In summary, the data presented here indicate that NYX-2925 is a novel pharmacological reagent that engages homeostatic plasticity. We found that NYX-2925 exhibits a dose-dependent mechanism of action; high concentrations *likely* activate ionotropic mechanisms whereas low concentrations *appear to* signal through the NMDAR in a metabotropic-like manner that increases synaptic levels of ionotropic glutamate receptors. Thus, NYX-2925 is a powerful tool to interrogate both canonical and unconventional modes of signaling through the NMDAR.

Statement of Interest

M.S. Bowers, L.P. Cacheaux, M.E. Schmidt, J.A. Sennello, K. Leaderbrand, M.A. Khan, R.A. Kroes, and J.R. Moskal are employees of Aptinyx, Inc., and have received financial compensation and stock options.

Author Contributions

Designed and synthesized NYX-783: MAK; Designed experiments: MSB, LPC, RAK, JRM; Ran experiments: MSB, LPC, MES, JAS, SUS; Analyzed and interpreted experiments: MSB, LPC, KL, SUS, RAK, JRM; Wrote the paper: MSB, LPC, KL, RAK, JRM

```
--Human subjects --
Involves human subjects:
If yes: Informed consent & ethics approval achieved:
=> if yes, please ensure that the info "Informed consent was achieved for all
subjects, and the experiments were approved by the local ethics committee." is
included in the Methods.


ARRIVE guidelines have been followed:
Yes
=> if it is a Review or Editorial, skip complete sentence => if No, include a
statement: "ARRIVE guidelines were not followed for the following reason:
"
(edit phrasing to form a complete sentence as necessary).
=> if Yes, insert "All experiments were conducted in compliance with the
ARRIVE guidelines." unless it is a Review or Editorial
```

Acknowledgements

The authors are extremely appreciative of expertise and resources provided by Nikon's Imaging Center for Advanced Microcopy at Northwestern University Feinberg School of Medicine (NCI CCSG P30 CA060553; NCRR 1S10 RR031680-01). We are also grateful for fruitful discussions with Robert M. Mitchell, PhD and graphical assistance from Rebecca J. Wilson.

Figure Legends

Figure 1. Experimental design for analysis of colocalization of GluN2-contianing NMDARs with PSD-95. a) Primary hippocampal neurons derived from E18 pups were cultured for 14 days prior to exchanging media with aCSF. Cells were allowed to recover in aCSF for 30 min at 37˚C. Next, NYX-2925, with or without 50 μM glutamate, was co-applied for either 30 or 60 min prior to processing cells for immunocytochemistry or proteomics. **b)** Representative dendrites immunolabeled of GluN2A and PSD-95. **c)** Representative dendrites immunolabeled for GluN2B and PSD-95. **d)** Representative immunolabeling of GluN2B and PSD-95 with computer-identified immunopositive puncta delineated. MAP2 was used as a marker for neurons and general index of cell health. Scale bar = 10 μm.

Figure 2. Quantification of colocalization of GluN2 with PSD-95. a) *Colocalization of GluN2A with PSD-95 was unaffected by NYX-2925 treatment in the presence 50 μM glutamate. n = 14 cells from 2 independent cell culture preparations (8 coverslips).* **b)** After incubating primary hippocampal neurons with various NYX-2925 concentrations in the presence of 50 μM glutamate, a significant increase in colocalization of GluN2B with PSD-95 was seen for 0.1 and 1 picomolar concentrations only. This NYX-2925-mediated increase in colocalization was blocked by the NMDAR glutamate site antagonist APV (*grey*). The antagonist APV was applied via both a 30 min pre-treatment as well as during the 30 min co-incubation with NYX-2925 and glutamate. No change in colocalization was observed if neurons were treated for 30 min with either 1 picomolar NYX-2925 *alone* (light gray) or 50 μM glutamate alone (dark gray). *n = 14 cells from 2 independent cell culture preparations (8 coverslips).* Whole-cell immunocontent of ***c*)** GluN2A, ***d*)** GluN2B, and ***e*)** PSD-95 were *decreased* after 30 min *incubation of NYX-2925 in the presence of 50 μM glutamate, but no difference was seen between either NYX-2925 concentration in the presence of 50 μM glutamate compared to glutamate alone. n = 5 – 9 independent cell culture preparations (whole-cell lysates).* ***f*)** No change in

colocalization of GluN2B with PSD-95 was observed after incubating neurons with *picomolar NYX-2925 concentrations* in the presence of 50 μM glutamate for 60 min*, but colocalization was decreased by continuous exposure to 30 nM NYX-2925 with 50 μM glutamate*. *n = 14 cells from 2 independent cell culture preparations (8 coverslips).* **g)** Representative dendrites immunolabeled for GluN2B and PSD-95. Scale bar = 10 μm. Veh: vehicle; Glu: glutamate. Data represent mean ± SEM ± *data spread; the line within each box represents the average, the box itself represents the SEM, and the whiskers indicate the spread of the data.* ** $p < 0.01$, ***$p < 0.001$ Tukey *post-hoc* analysis, n = 14 cells per treatment; **** $p < 0.0001$ Dunnett's *post-hoc* analysis.

Figure 3. NYX-2925 mediates GluN2B colocalization with PSD-95 via a metabotropic-like mechanism. Neurons were treated as before with NYX-2925 and glutamate and the effect of NMDAR blockers on GluN2B colocalization with PSD-95 quantified. **a)** Co-application of 1 picomolar NYX-2925 with 50 μM glutamate increased colocalization of GluN2B with PSD-95, and this effect was blocked by the glutamate site antagonist APV. In contrast, significantly increased colocalization was observed when either the channel blocker MK-801 or the glycine site antagonist 7CK were applied. As before, antagonists were both applied before and during NYX-2925/glutamate incubation. Colocalization was not different from control conditions following application of these antagonists with glutamate alone (in the absence of NYX-2925; dark grey) or with NYX-2925 alone (light grey). n = 14 – 28 cells per treatment *from 2 independent cell culture preparations (8 coverslips).* **b)** Representative dendrites immunolabeled for GluN2B and PSD-95. **c)** Effects of NYX-2925 on calcium transients following NMDAR activation. Primary *hippocampal* neurons were loaded with Fluo-4-AM, and calcium imaging performed. After a baseline measurement, 4 μM NMDA was washed onto the cells for 1 min followed by a 2 min washout. NYX-2925 + NMDA was then washed onto the cells to determine if NYX-2925 enhanced NMDA receptor mediated calcium transients. Two *independent culture preparations* were used (n = 6 cover slips). Scale bar = 10 μm. Data represent mean ± SEM ± *data spread; the line within each box represents the average, the box itself represents the SEM, and*

the whiskers indicate the spread of the data. ****p < 0.0001 Student's t-Test; ***p < 0.001 Tukey *post-hoc* analysis; *** p < 0.01 Tukey post-hoc analysis,* *p < 0.05 Fisher *post-hoc* analysis.

Figure 4. NYX-2925 pre-treatment facilitates chemLTP-mediated synaptic GluA1 recruitment. a) As before, neurons (14 days *in vitro*) were changed to aCSF and allowed to recover for 30 min at 37˚C. Next, cells were co-treated with 1 picomolar NYX-2925 and 50 μM glutamate and colocalization of GluA1-containing AMPARs with PSD-95 quantified. Cells from the same cultures underwent chemLTP stimulation following NYX-2925/glutamate pre-treatment. **b – d)** Representative cellular immunolabeling of GluA1 and PSD-95. **b' – d')** Representative dendrites immunolabeled for GluA1 and PSD-95. **e)** Co-incubation with *1 pM* NYX-2925 and glutamate in the absence of chemLTP did not affect colocalization of GluA1 with PSD-95. **f)** chemLTP stimulation increased colocalization, and this effect was facilitated by *1 pM* NYX-2925/glutamate pre-treatment. Veh: vehicle. Scale bar = 10 μm. Data represent mean ± SEM *± data spread; the line within each box represents the average, the box itself represents the SEM, and the whiskers indicate the spread of the data.* ***p < 0.001, *** p < 0.01, *p < 0.05* Tukey *post-hoc* analysis, n = 14 cells per treatment *from 2 independent cell culture preparations (8 coverslips).*

Figure 5. Pharmacokinetic model of NYX-2925-mediated metaplasticity. Cartoon depicting absorption, metabolism, and elimination of NYX-2925. Following *an oral* drug bolus, central levels of NYX-2925 raise into the concentration range *(~ 44 nanomolar within ~ 1 h)* that facilitates LTP *in vivo* (Khan et al., 2018). With time *(> 8 h)*, drug concentrations fall into the range where homeostatic plasticity is observed *(low picomolar)*, which may account for both the rapid and long-lasting effects of drug seen *in vivo* following a single treatment. *Thus, at some point, brain NYX-2925 concentrations fall within both the ionotropic and putative metabotropic ranges after oral dosing.*

Table 1. Ontological analysis of differentially expressed hippocampal proteins following treatment with NYX-2925 (1 pM/30 min). Proteins within each pathway that are up-regulated by NYX-2925 are depicted in **red**. Proteins within each pathway that are down-regulated by NYX-2925 are depicted in **green**.

Receptor trafficking

Ingenuity Canonical Pathways	p-value	Molecules
Clathrin-mediated Endocytosis Signaling	3.467E-04	**MYO6, EPHB2, AP2B1, PPP3R1, ARPC5, RPS27A, STAM, TSG101**

Synaptic plasticity

Ingenuity Canonical Pathways	p-value	Molecules
EIF2 Signaling	9.333E-10	**EIF3C, RPS23, RPL30, RPS11, RPS6, EIF3F, RPS4Y1, EIF4G2, HNRNPA1, MAPK3, RPS9, EIF3A, RPS27A, RPL6, RPS12**
Regulation of eIF4 and p70S6K Signaling	1.230E-08	**RPS6, EIF3F, EIF3C, RPS4Y1, EIF4G2, MAPK3, RPS23, RPS9, EIF3A, RPS27A, RPS12, RPS11**
mTOR Signaling	2.239E-08	**RPS6, EIF3F, EIF3C, RHEB, RPS4Y1, EIF4G2, MAPK3, RPS23, RPS9, EIF3A, RPS27A, RPS12, RPS11**
Calcium Signaling	7.943E-05	**CAMK1, PRKAR2B, Calm1 (includes others), MAPK3, PPP3R1, CAMKK1, Tpm1, CACNB3, Tpm3**
Sirtuin Signaling Pathway	0.0040	**NDUFB4, NDUFA5, Hist1h1e, ATP5D, MAPK3, ATG3, SMARCA5, NDUFA8**
Synaptic Long Term Potentiation	0.0214	**PRKAR2B, Calm1 (includes others), MAPK3, PPP3R1**

Synaptic transmission

Ingenuity Canonical Pathways	p-value	Molecules
Protein Kinase A Signaling	1.86E-06	**AKAP5, MYH10, HIST1H1C, Calm1 (includes others), YWHAE, PPP1CB, CDC23, PLCH2, GNB4, Hist1h1e, CAMK2D, CAMK2A, MAP2K2, PPP1R12A, MAPK3, PRKACA, HIST1H1D, MAP2K1, VASP, CAMK2G**
Calcium Signaling	7.943E-05	**CAMK1, PRKAR2B, Calm1 (includes others), MAPK3, PPP3R1, CAMKK1, Tpm1, CACNB3, Tpm3**
nNOS Signaling in Neurons	0.0078	**CAPNS1, Calm1 (includes others), PPP3R1**
cAMP-mediated signaling	0.0141	**CAMK1, PRKAR2B, Calm1 (includes others), MAPK3, CNR1, PPP3R1**
PI3K Signaling	0.0263	**CD81, Calm1 (includes others), MAPK3, PPP3R1**

Synaptic remodeling

Ingenuity Canonical Pathways	p-value	Molecules
Netrin Signaling	0.0024	**PRKAR2B, PPP3R1, ABLIM2, CACNB3**

Androgen Signaling	0.0309	**PRKAR2B, Calm1 (includes others), MAPK3, CACNB3**
Neuregulin Signaling	0.0407	**RPS6, PICK1, MAPK3**

Synaptogenesis

Ingenuity Canonical Pathways	**p-value**	**Molecules**
Corticotropin Releasing Hormone Signaling	0.0013	**PRKAR2B, Calm1 (includes others), MAPK3, CNR1, ARPC5, CACNB3**
Netrin Signaling	0.0024	**PRKAR2B, PPP3R1, ABLIM2, CACNB3**
RhoA Signaling	0.0229	**ARHGEF12, SEPT9, SEPT3, ARPC5**
PI3K Signaling	0.0263	**CD81, Calm1 (includes others), MAPK3, PPP3R1**

Regulation of gene expression

Ingenuity Canonical Pathways	**p-value**	**Molecules**
EIF2 Signaling	9.333E-10	**EIF3C, RPS23, RPL30, RPS11, RPS6, EIF3F, RPS4Y1, EIF4G2, HNRNPA1, MAPK3, RPS9, EIF3A, RPS27A, RPL6, RPS12**
Regulation of eIF4 and p70S6K Signaling	1.230E-08	**RPS6, EIF3F, EIF3C, RPS4Y1, EIF4G2, MAPK3, RPS23, RPS9, EIF3A, RPS27A, RPS12, RPS11**
DNA Methylation and Transcriptional Repression Signaling	0.0347	**CHD4, MBD3**

Table 2. Ontological analysis of differentially expressed hippocampal proteins following treatment with NYX-2925 (30 nM/30 min). Proteins within each pathway that are up-regulated by NYX-2925 are depicted in **red**. Proteins within each pathway that are down-regulated by NYX-2925 are depicted in **green**.

Receptor trafficking

CDK5 Signaling	1.00E-04	**MAP2K2, PPP1R12A, MAPK3, MAPT, PPP2R5D, PRKACA, PPP1CB, MAP2K1**
14-3-3-mediated Signaling	1.29E-04	**AKT1, YWHAE, MAP2K2, MAPK3, MAPT, PLCH2, MAP2K1, SNCA, AKT1S1**
Protein Ubiquitination Pathway	0.0158	**PSMD11, USP47, UBE2K, USP19, CDC23, PSMA3, PRKN, PSMD4, DNAJB2**

Synaptic plasticity

Synaptic Long Term Potentiation	2.69E-08	**Calm1 (includes others), GRIA1, PPP1CB, PLCH2, CAMK2D, CAMK2A, PPP1R12A, MAP2K2, MAPK3, PRKACA, MAP2K1, GRIA3, CAMK2G**
Sirtuin Signaling Pathway	1.48E-06	**NDUFV1, HIST1H1C, NDUFB4, NDRG1, ATG3, G6PD, NDUFB8, ARG2, Hist1h1e, AKT1, NDUFV2, ATG9A, MAPK3, NDUFA6, NDUFA12, HIST1H1D, NDUFA8**
Calcium Signaling	1.07E-05	**MYH10, AKAP5, Calm1 (includes others), GRIA1, Tpm1, CACNA1E, CAMK2D, CAMK2A, MAPK3, CAMKK1, PRKACA, GRIA3, CAMK2G**
EIF2 Signaling	1.00E-04	**AKT1, RPS20, MAP2K2, MAPK3, Rpl36a, RPS9, RPL30, RPL19, PPP1CB, EIF2S1, MAP2K1, RPL10A**
Synaptic Long Term Depression	0.0010	**PLA2G6, CACNA1E, MAP2K2, MAPK3, PPP2R5D, GRIA1, PLCH2, MAP2K1, GRIA3**
Regulation of eIF4 and p70S6K Signaling	0.0021	**AKT1, RPS20, MAP2K2, MAPK3, PPP2R5D, RPS9, EIF2S1, MAP2K1**
mTOR Signaling	0.0282	**AKT1, RPS20, MAPK3, PPP2R5D, RPS9, FNBP1, AKT1S1**

Synaptic transmission

Protein Kinase A Signaling	1.86E-06	**AKAP5, MYH10, HIST1H1C, Calm1 (includes others), YWHAE, PPP1CB, CDC23, PLCH2, GNB4, Hist1h1e, CAMK2D, CAMK2A, MAP2K2, PPP1R12A, MAPK3, PRKACA, HIST1H1D, MAP2K1, VASP, CAMK2G**
CREB Signaling in Neurons	2.95E-06	**Calm1 (includes others), GRIA1, PLCH2, GNB4, CACNA1E, AKT1, CAMK2D, CAMK2A, MAP2K2, MAPK3, PRKACA, MAP2K1, GRIA3, CAMK2G**
Calcium Signaling	1.07E-05	**MYH10, AKAP5, Calm1 (includes others), GRIA1, Tpm1, CACNA1E, CAMK2D, CAMK2A, MAPK3, CAMKK1, PRKACA, GRIA3, CAMK2G**
Signaling by Rho Family GTPases	3.39E-04	**STMN1, GNB4, SEPT5, MAP2K2, PPP1R12A, MAPK3, ARHGEF7, ARPC2, SEPT7, SEPT11, MAP2K1, FNBP1**
cAMP-mediated signaling	5.13E-04	**AKAP5, CAMK2A, CAMK2D, Calm1 (includes others), MAP2K2, RAP1GAP, MAPK3, CNR1, PRKACA, MAP2K1, CAMK2G**

p70S6K Signaling	7.08E-04	**AKT1, YWHAE, MAP2K2, MAPK3, MAPT, PPP2R5D, PLCH2, MAP2K1**
ERK/MAPK Signaling	7.24E-04	**PLA2G6, MAP2K2, PPP1R12A, MAPK3, PPP2R5D, PRKACA, PPP1CB, CRK, MAP2K1, KSR1**
Ephrin Receptor Signaling	0.0011	**GNB4, AKT1, ABI1, MAP2K2, ITSN1, MAPK3, ARPC2, CRK, MAP2K1**
PI3K/AKT Signaling	0.0100	**AKT1, YWHAE, MAP2K2, MAPK3, PPP2R5D, MAP2K1**
Glutamate Receptor Signaling	0.0500	**Calm1 (includes others), GRIA1, GRIA3**

Synaptic remodeling

Signaling by Rho Family GTPases	3.39E-04	**STMN1, GNB4, SEPT5, MAP2K2, PPP1R12A, MAPK3, ARHGEF7, ARPC2, SEPT7, SEPT11, MAP2K1, FNBP1**
Actin Cytoskeleton Signaling	0.0062	**MYH10, MAP2K2, PPP1R12A, MAPK3, ARHGEF7, ARPC2, PPP1CB, CRK, MAP2K1**
Axonal Guidance Signaling	0.0068	**ITSN1, ARHGEF7, CRK, PLCH2, GNB4, SRGAP3, AKT1, MAP2K2, MAPK3, ARPC2, PRKACA, MAP2K1, VASP, FARP2**
Actin Nucleation by ARP-WASP Complex	0.0089	**PPP1R12A, ARPC2, FNBP1, VASP**
Regulation of Actin-based Motility by Rho	0.0427	**PPP1R12A, ARPC2, PPP1CB, FNBP1**

Synaptogenesis

Integrin Signaling	3.80E-04	**AKT1, MAP2K2, PPP1R12A, MAPK3, ARHGEF7, ARPC2, PPP1CB, CRK, MAP2K1, FNBP1, VASP**
ERK/MAPK Signaling	7.24E-04	**PLA2G6, MAP2K2, PPP1R12A, MAPK3, PPP2R5D, PRKACA, PPP1CB, CRK, MAP2K1, KSR1**
Corticotropin Releasing Hormone Signaling	0.0043	**CACNA1E, Calm1 (includes others), MAP2K2, MAPK3, CNR1, PRKACA, MAP2K1**
IGF-1 Signaling	0.0046	**AKT1, YWHAE, MAP2K2, MAPK3, PRKACA, MAP2K1**
RhoA Signaling	0.0095	**SEPT5, PPP1R12A, ARPC2, SEPT7, PPP1CB, SEPT11**
PI3K/AKT Signaling	0.0100	**AKT1, YWHAE, MAP2K2, MAPK3, PPP2R5D, MAP2K1**

Regulation of gene expression

EIF2 Signaling	1.00E-04	**AKT1, RPS20, MAP2K2, MAPK3, Rpl36a, RPS9, RPL30, RPL19, PPP1CB, EIF2S1, MAP2K1, RPL10A**
Regulation of eIF4 and p70S6K Signaling	0.0021	**AKT1, RPS20, MAP2K2, MAPK3, PPP2R5D, RPS9, EIF2S1, MAP2K1**

Literature Cited

Abraham, W. C. (2008) Metaplasticity: tuning synapses and networks for plasticity. Nat Rev Neurosci, 9, 387.

Abraham, W. C., Bear, M. F. (1996) Metaplasticity: the plasticity of synaptic plasticity. Trends Neurosci, 19, 126–130.

Ahmad, M., Polepalli, J. S., Goswami, D., Yang, X., Kaeser-Woo, Y. J., Südhof, T. C., Malenka, R. C. (2012) Postsynaptic complexin controls AMPA receptor exocytosis during LTP. Neuron, 73, 260–267.

Aiyer, R., Mehta, N., Gungor, S., Gulati, A. (2017) A Systematic Review of NMDA Receptor Antagonists for Treatment of Neuropathic Pain in Clinical Practice. Clin J Pain,

Al-Hallaq, R. A., Conrads, T. P., Veenstra, T. D., Wenthold, R. J. (2007) NMDA di-heteromeric receptor populations and associated proteins in rat hippocampus. J Neurosci, 27, 8334–8343.

Babiec, W. E., Guglietta, R., Jami, S. A., Morishita, W., Malenka, R. C., O'Dell, T. J. (2014) Ionotropic NMDA receptor signaling is required for the induction of long-term depression in the mouse hippocampal CA1 region. J Neurosci, 34, 5285–5290.

Bard, L., Sainlos, M., Bouchet, D., Cousins, S., Mikasova, L., Breillat, C., Stephenson, F. A., Imperiali, B., Choquet, D., Groc, L. (2010) Dynamic and specific interaction between synaptic NR2-NMDA receptor and PDZ proteins. Proc Natl Acad Sci U S A, 107, 19561–19566.

Barria, A., Malinow, R. (2002) Subunit-specific NMDA receptor trafficking to synapses. Neuron, 35, 345–353.

Barria, A., Malinow, R. (2005) NMDA receptor subunit composition controls synaptic plasticity by regulating binding to CaMKII. Neuron, 48, 289–301.

Bliss, T. V., Collingridge, G. L. (1993) A synaptic model of memory: long-term potentiation in the hippocampus. Nature, 361, 31–39.

Chen, H. S., Lipton, S. A. (2006) The chemical biology of clinically tolerated NMDA receptor antagonists. J Neurochem, 97, 1611–1626.

Chung, C., Wu, W. H., Chen, B. S. (2015) Identification of Novel 14-3-3 Residues That Are Critical for Isoform-specific Interaction with GluN2C to Regulate N-Methyl-D-aspartate (NMDA) Receptor Trafficking. J Biol Chem, 290, 23188–23200.

Cox, J., Neuhauser, N., Michalski, A., Scheltema, R. A., Olsen, J. V., Mann, M. (2011) Andromeda: a peptide search engine integrated into the MaxQuant environment. J Proteome Res, 10, 1794–1805.

Crump, F. T., Dillman, K. S., Craig, A. M. (2001) cAMP-dependent protein kinase mediates activity-regulated synaptic targeting of NMDA receptors. J Neurosci, 21, 5079–5088.

Cull-Candy, S. G., Leszkiewicz, D. N. (2004) Role of distinct NMDA receptor subtypes at central synapses. Sci STKE, 2004, re16.

Dalva, M. B., Takasu, M. A., Lin, M. Z., Shamah, S. M., Hu, L., Gale, N. W., Greenberg, M. E. (2000) EphB receptors interact with NMDA receptors and regulate excitatory synapse formation. Cell, 103, 945–956.

Dore, K., Aow, J., Malinow, R. (2015) Agonist binding to the NMDA receptor drives movement of its cytoplasmic domain without ion flow. Proc Natl Acad Sci U S A, 112, 14705–14710.

Dore, K., Stein, I. S., Brock, J. A., Castillo, P. E., Zito, K., Sjöström, P. J. (2017) Unconventional NMDA Receptor Signaling. J Neurosci, 37, 10800–10807.

Dubocovich, M. L. (1983) Melatonin is a potent modulator of dopamine release in the retina. Nature, 306, 782–784.

Elias, G. M., Nicoll, R. A. (2007) Synaptic trafficking of glutamate receptors by MAGUK scaffolding proteins. Trends Cell Biol, 17, 343–352.

Ferreira, J. S., Papouin, T., Ladépêche, L., Yao, A., Langlais, V. C., Bouchet, D., Dulong, J., Mothet, J. P., Sacchi, S., Pollegioni, L., Paoletti, P., Oliet, S. H. R., Groc, L. (2017) Co-agonists differentially tune GluN2B-NMDA receptor trafficking at hippocampal synapses. Elife, 6,

Fong, D. K., Rao, A., Crump, F. T., Craig, A. M. (2002) Rapid synaptic remodeling by protein kinase C: reciprocal translocation of NMDA receptors and calcium/calmodulin-dependent kinase II. J

Neurosci, 22, 2153–2164.

Fujii, S., Tanaka, H., Hirano, T. (2018) Suppression of AMPA Receptor Exocytosis Contributes to Hippocampal LTD. J Neurosci, 38, 5523–5537.

Furuyashiki, T., Fujisawa, K., Fujita, A., Madaule, P., Uchino, S., Mishina, M., Narumiya, S. (1999) Citron, a rho-target, interacts with PSD-95/SAP-90 at glutamatergic synapses in the thalamus. J Neurosci, 19, 109–18.

Gardoni, F., Picconi, B., Ghiglieri, V., Polli, F., Bagetta, V., Bernardi, G., Cattabeni, F., Di Luca, M., Calabresi, P. (2006) A critical interaction between NR2B and MAGUK in L-DOPA induced dyskinesia. J Neurosci, 26, 2914–2922.

Ghasemi, M., Phillips, C., Fahimi, A., McNerney, M. W., Salehi, A. (2017) Mechanisms of action and clinical efficacy of NMDA receptor modulators in mood disorders. Neurosci Biobehav Rev, 80, 555–572.

Ghoreishi-Haack, N., Priebe, J.M., Aguado, J.D., Colechio, E.M., Burgdorf, J.S., Bowers, M.S., Cearley, C.N., Khan, M.A., Moskal, J.R. (2018) NYX-2925 is a novel N-methyl-D-aspartate receptor modulator that induces rapid and long-lasting analgesia in rat models of neuropathic pain. JPET. 366, 485-497.

Gielen, M., Siegler Retchless, B., Mony, L., Johnson, J. W., Paoletti, P. (2009) Mechanism of differential control of NMDA receptor activity by NR2 subunits. Nature, 459, 703–707.

Guillaud. L., Setou, M., Hirokawa, N. (2003) KIF17 dynamics and regulation of NR2B trafficking in hippocampal neurons. J Neurosci. 23, 131.

Groc, L., Bard, L., Choquet, D. (2009) Surface trafficking of N-methyl-D-aspartate receptors: physiological and pathological perspectives. Neuroscience, 158, 4–18.

Groc, L., Choquet, D. (2006) AMPA and NMDA glutamate receptor trafficking: multiple roads for reaching and leaving the synapse. Cell Tissue Res, 326, 423–438.

Groc, L., Heine, M., Cognet, L., Brickley, K., Stephenson, F. A., Lounis, B., Choquet, D. (2004) Differential activity-dependent regulation of the lateral mobilities of AMPA and NMDA

receptors. Nat Neurosci, 7, 695–696.

Groc, L., Heine, M., Cousins, S. L., Stephenson, F. A., Lounis, B., Cognet, L., Choquet, D. (2006) NMDA receptor surface mobility depends on NR2A-2B subunits. Proc Natl Acad Sci U S A, 103, 18769–18774.

Hansen, K. B., Ogden, K. K., Yuan, H., Traynelis, S. F. (2014) Distinct functional and pharmacological properties of Triheteromeric GluN1/GluN2A/GluN2B NMDA receptors. Neuron, 81, 1084–1096.

Harris, A. Z., Pettit, D. L. (2007) Extrasynaptic and synaptic NMDA receptors form stable and uniform pools in rat hippocampal slices. J Physiol, 584, 509–519.

Ishii, T., Moriyoshi, K., Sugihara, H., Sakurada, K., Kadotani, H., Yokoi, M., Akazawa, C., Shigemoto, R., Mizuno, N., Masu, M. (1993) Molecular characterization of the family of the N-methyl-D-aspartate receptor subunits. J Biol Chem, 268, 2836–2843.

Kessels, H. W., Nabavi, S., Malinow, R. (2013) Metabotropic NMDA receptor function is required for β-amyloid-induced synaptic depression. Proc Natl Acad Sci U S A, 110, 4033–4038.

Kew, J. N., Richards, J. G., Mutel, V., Kemp, J. A. (1998) Developmental changes in NMDA receptor glycine affinity and ifenprodil sensitivity reveal three distinct populations of NMDA receptors in individual rat cortical neurons. J Neurosci, 18, 1935–1943.

Khan, M. A., Houck, D. R., Gross, A. L., Zhang, X. L., Cearley, C., Madsen, T. M., Kroes, R. A., Stanton, P. K., Burgdorf, J., Moskal, J. R. (2018) NYX-2925 is a novel NMDA receptor-specific spirocyclic-β-lactam that modulates synaptic plasticity processes associated with learning and memory. Int J Neuropsychopharmacol, 21, 242–254.

Kim, Y., Hsu, C. L., Cembrowski, M. S., Mensh, B. D., Spruston, N. (2015) Dendritic sodium spikes are required for long-term potentiation at distal synapses on hippocampal pyramidal neurons. Elife, 4, 1-30.

Kneussel, M., Wagner, W. (2013) Myosin motors at neuronal synapses: drivers of membrane transport and actin dynamics. Nat Rev Neurosci. 14, 233-47.

Krämer, A., Green, J., Pollard, J., Tugendreich, S. (2014) Causal analysis approaches in Ingenuity

Pathway Analysis. Bioinformatics, 30, 523–530.

Krystal, J. H., Abdallah, C. G. , Averill, L. A. Kelmendi, B., Harpaz-Rotem, I., Sanacora, G., Southwick, S. M., Duman, R. S. (2017) Synaptic loss and the pathophysiology of PTSD: Implications for ketamine as a prototype novel therapeutic. Curr Psych Rep, 74, 1 - 11.

Kumar, A. (2015) NMDA Receptor Function During Senescence: Implication on Cognitive Performance. Front Neurosci, 9, 473.

Lan, J. Y., Skeberdis, V. A., Jover, T., Grooms, S. Y., Lin, Y., Araneda, R. C., Zheng, X., Bennett, M. V., Zukin, R. S. (2001) Protein kinase C modulates NMDA receptor trafficking and gating. Nat Neurosci, 4, 382–390.

Lau, C. G., Zukin, R. S. (2007) NMDA receptor trafficking in synaptic plasticity and neuropsychiatric disorders. Nat Rev Neurosci, 8, 413–426.

Lavezzari, G., McCallum, J., Dewey, C. M., Roche, K. W. (2004) Subunit-specific regulation of NMDA receptor endocytosis. J Neurosci, 24, 6383–6391.

Lavezzari, G., McCallum, J., Lee, R., Roche, K. W. (2003) Differential binding of the AP-2 adaptor complex and PSD-95 to the C-terminus of the NMDA receptor subunit NR2B regulates surface expression. Neuropharmacology, 45, 729–737.

Lisman, J., Yasuda, R., Raghavachari, S. (2012) Mechanisms of CaMKII action in long-term potentiation. Nat Rev Neurosci, 13, 169–182.

Liu, X. B., Murray, K. D., Jones, E. G. (2004) Switching of NMDA receptor 2A and 2B subunits at thalamic and cortical synapses during early postnatal development. J Neurosci, 24, 8885–8895.

Lu, W., Man, H., Ju, W., Trimble, W. S., MacDonald, J. F., Wang, Y. T. (2001) Activation of synaptic NMDA receptors induces membrane insertion of new AMPA receptors and LTP in cultured hippocampal neurons. Neuron, 29, 243–254.

Luo, J., Wang, Y., Yasuda, R. P., Dunah, A. W., Wolfe, B. B. (1997) The majority of N-methyl-D-aspartate receptor complexes in adult rat cerebral cortex contain at least three different subunits (NR1/NR2A/NR2B). Mol Pharmacol, 51, 79–86.

Luo, J. H., Rotterdam, H. (1997) Primary amyloid tumor of the breast: a case report and review of the literature. Mod Pathol, 10, 735–738.

Montes de Oca Balderas, P. (2018) Flux-independent NDMAR signaling: molecular mediators, cellular functions, and complexities. Int J Mol Sci. 19, 3800, 1-22.

Monyer, H., Burnashev, N., Laurie, D. J., Sakmann, B., Seeburg, P. H. (1994) Developmental and regional expression in the rat brain and functional properties of four NMDA receptors. Neuron, 12, 529–540.

Monyer, H., Sprengel, R., Schoepfer, R., Herb, A., Higuchi, M., Lomeli, H., Burnashev, N., Sakmann, B., Seeburg, P. H. (1992) Heteromeric NMDA receptors: molecular and functional distinction of subtypes. Science, 256, 1217–1221.

Moskal, J. R., Burgdorf, J. S., Stanton, P. K., Kroes, R. A., Disterhoft, J. F., Burch, R. M., Khan, M. A. (2017) The Development of Rapastinel (Formerly GLYX-13); A Rapid Acting and Long Lasting Antidepressant. Curr Neuropharmacol, 15, 47–56.

Münnich, S., Taft, M.H., Manstein, D.J. (2014) Crytal structure of human myosin 1c—the motor in GLUT4 exocytosis: implications for Ca2+ regulation and 14-3-3 binding. J Mol Biol, 426, 2070-81.

Nabavi, S., Kessels, H. W., Alfonso, S., Aow, J., Fox, R., Malinow, R. (2013) Metabotropic NMDA receptor function is required for NMDA receptor-dependent long-term depression. Proc Natl Acad Sci U S A, 110, 4027–4032.

Nault, F., De Koninck, P. (2010) Dissociated Hippocampal Cultures. In: Protocols for Neural Cell Culture: Fourth Edition (Doering, L. C., ed), pp 137–159. Totowa, NJ: Humana Press.

Ng, T. I., Krishnan, P., Pilot-Matias, T., Kati, W., Schnell, G., Beyer, J., Reisch, T., Lu, L., Dekhtyar, T., Irvin, M., Tripathi, R., Maring, C., Randolph, J. T., Wagner, R., Collins, C. (2017) Antimicrob Agents Chemother, 61,

Nong, Y., Huang, Y. Q., Ju, W., Kalia, L. V., Ahmadian, G., Wang, Y. T., Salter, M. W. (2003) Glycine binding primes NMDA receptor internalization. Nature, 422, 302–307.

Ohashi, R., Takao, K., Miyakawa, T., Shiina, N. (2016) Comprehensive behavioral analysis of RNG105

(Caprin1) heterozygous mice: Reduced social interaction and attenuated response to novelty. Sci Rep, 6, 20775.

Okamoto, K., Nagai, T., Miyawaki, A., Hayashi, Y. (2004) Rapid and persistent modulation of actin dynamics regulates postsynaptic reorganization underlying bidirectional plasticity. Nat Neurosci. 7, 1104-12.

Paoletti, P. (2011) Molecular basis of NMDA receptor functional diversity. Eur J Neurosci, 33, 1351–1365.

Pérez-Otaño, I., Ehlers, M. D. (2005) Homeostatic plasticity and NMDA receptor trafficking. Trends Neurosci, 28, 229–238.

Petralia, R. S., Al-Hallaq, R., A., Wenthold, R., J. (2009) Trafficking and targeting of NMDA receptors. In: Biology of the NMDA receptor (Van Dongen, A., NM. ed), cp 8. Boca Raton, FL: CRC Press.

Petralia, R. S., Wang, Y. X., Hua, F., Yi, Z., Zhou, A., Ge, L., Stephenson, F. A., Wenthold, R. J. (2010) Organization of NMDA receptors at extrasynaptic locations. Neuroscience, 167, 68–87.

Prybylowski, K., Chang, K., Sans, N., Kan, L., Vicini, S., Wenthold, R. J. (2005) The synaptic localization of NR2B-containing NMDA receptors is controlled by interactions with PDZ proteins and AP-2. Neuron, 47, 845–857.

Raiteri, L., Luccini, E., Romei, C., Salvadori, S., Calò, G. (2009) Neuropeptide S selectively inhibits the release of 5-HT and noradrenaline from mouse frontal cortex nerve endings. Br J Pharmacol, 157, 474–481.

Rauner, C., Köhr, G. (2011) Triheteromeric NR1/NR2A/NR2B receptors constitute the major N-methyl-D-aspartate receptor population in adult hippocampal synapses. J Biol Chem, 286, 7558–7566.

Roche, K. W., Standley, S., McCallum, J., Dune Ly, C., Ehlers, M. D., Wenthold, R. J. (2001) Molecular determinants of NMDA receptor internalization. Nat Neurosci, 4, 794–802.

Romberg, C., Raffel, J., Martin, L., Sprengel, R., Seeburg, P. H., Rawlins, J. N., Bannerman, D. M., Paulsen, O. (2009) Induction and expression of GluA1 (GluR-A)-independent LTP in the

hippocampus. Eur J Neurosci, 29, 1141–1152.

Sanderson, J. L., Gorski, J. A., Dell'Acqua, M. L. (2016) NMDA Receptor-Dependent LTD Requires Transient Synaptic Incorporation of Ca^{2+}-Permeable AMPARs Mediated by AKAP150-Anchored PKA and Calcineurin. Neuron, 89, 1000–1015.

Scimemi, A., Fine, A., Kullmann, D.M., Rusakov, D.A. (2004) NR2B-containing receptor mediate cross talk among hippocampal synapses. J Neurosci, 24, 4767-4777.

Sheng, M., Cummings, J., Roldan, L. A., Jan, Y. N., Jan, L. Y. (1994) Changing subunit composition of heteromeric NMDA receptors during development of rat cortex. Nature, 368, 144–147.

Sheng, M., Hoogenraad, C. C. (2007) The postsynaptic architecture of excitatory synapses: a more quantitative view. Annu Rev Biochem, 76, 823–847.

Shi, S., Hayashi, Y., Esteban, J. A., Malinow, R. (2001) Subunit-specific rules governing AMPA receptor trafficking to synapses in hippocampal pyramidal neurons. Cell, 105, 331–343.

Siebler, M., Köller, H., Stichel, C. C., Müller, H. W., Freund, H. J. (1993) Spontaneous activity and recurrent inhibition in cultured hippocampal networks. Synapse, 14, 206–213.

Stein, I. S., Gray, J. A., Zito, K. (2015) Non-Ionotropic NMDA Receptor Signaling Drives Activity-Induced Dendritic Spine Shrinkage. J Neurosci, 35, 12303–12308.

Tamburri, A., Dudilot, A., Licea, S., Bourgeois, C., Boehm, J. (2013) NMDA-receptor activation but not ion flux is required for amyloid-beta induced synaptic depression. PLoS One, 8, e65350.

Thomas, C. G., Miller, A. J., Westbrook, G. L. (2006) Synaptic and extrasynaptic NMDA receptor NR2 subunits in cultured hippocampal neurons. J Neurophysiol, 95, 1727–1734.

Thorton, C., Yaka, R., Dinh, S., Ron, D. (2003) H-Ras modulates N-methyl-D-aspartate receptor function via inhibition of Src tyrosine kinase activity. JBC, 278, 23823 – 23929.

Tovar, K. R., Westbrook, G. L. (1999) The incorporation of NMDA receptors with a distinct subunit composition at nascent hippocampal synapses in vitro. J Neurosci, 19, 4180–4188.

Tovar, K. R., Westbrook, G. L. (2002) Mobile NMDA receptors at hippocampal synapses. Neuron, 34, 255–264.

Traynelis, S. F., Wollmuth, L. P., McBain, C. J., Menniti, F. S., Vance, K. M., Ogden, K. K., Hansen, K. B., Yuan, H., Myers, S. J., Dingledine, R. (2010) Glutamate receptor ion channels: structure, regulation, and function. Pharmacol Rev, 62, 405–496.

Trepanier, C. H., Jackson, M. F., MacDonald, J. F. (2012) Regulation of NMDA receptors by the tyrosine kinase Fyn. FEBS J, 279, 12–19.

van Zundert, B., Yoshii, A., Constantine-Paton, M. (2004) Receptor compartmentalization and trafficking at glutamate synapses: a developmental proposal. Trends Neurosci, 27, 428–437.

Vicini, S., Wang, J. F., Li, J. H., Zhu, W. J., Wang, Y. H., Luo, J. H., Wolfe, B. B., Grayson, D. R. (1998) Functional and pharmacological differences between recombinant N-methyl-D-aspartate receptors. J Neurophysiol, 79, 555–566.

Vissel, B., Krupp, J. J., Heinemann, S. F., Westbrook, G. L. (2001) A use-dependent tyrosine dephosphorylation of NMDA receptors is independent of ion flux. Nat Neurosci, 4, 587–596.

Volianskis, A., France, G., Jensen, M. S., Bortolotto, Z. A., Jane, D. E., Collingridge, G. L. (2015) Long-term potentiation and the role of N-methyl-D-aspartate receptors. Brain Res, 1621, 5–16.

Wenthold, R. J., Prybylowski, K., Standley, S., Sans, N., Petralia, R. S. (2003) Trafficking of NMDA receptors. Annu Rev Pharmacol Toxicol, 43, 335–358.

Yang, L., Mao, L., Tang, Q., Samdani, S., Liu, Z., Wang, J. Q. (2004) A novel Ca2+-independent signaling pathway to extracellular signal-regulated protein kinase by coactivation of NMDA receptors and metabotropic glutamate receptor 5 in neurons. J Neurosci, 24, 10846–10857.

Yuan, H., Hansen, K. B., Vance, K. M., Ogden, K. K., Traynelis, S. F. (2009) Control of NMDA receptor function by the NR2 subunit amino-terminal domain. J Neurosci, 29, 12045–12058.

Yunfei, B., Wang, N., Wang, S., Sheng, T., Tian, T., Chen, L., Pan, W., Zhu, M., Luo, J., Lu, W. (2015) Myosin IIb-dependent regulation of actin dynamics is required for N-methyl-D-aspartate receptor trafficking during synaotic plasticity. JBC, 290, 25395 – 25410.

Zamanillo, D., Sprengel, R., Hvalby, O., Jensen, V., Burnashev, N., Rozov, A., Kaiser, K. M., Köster, H. J., Borchardt, T., Worley, P., Lübke, J., Frotscher, M., Kelly, P. H., Sommer, B., Andersen, P.,

Seeburg, P. H., Sakmann, B. (1999) Importance of AMPA receptors for hippocampal synaptic plasticity but not for spatial learning. Science, 284, 1805–1811.

Zhang, S., Edelmann, L., Liu, J., Crandall, J.E., Morabito, M.A. (2008), Cdk5 regulates the phosphorylation of tyrosine 1472 NR2B and the surface expression of NMDA receptors. J Neurosci, 28, 415-24.

Zhang, W., Vasquez, L., Apperson, M., Kennedy, M. B. (1999) Citron binds to PSD-95 at glutamatergic synapses on inhibitory neurons in the hippocampus. J Neurosci, 19, 96–108.

Zhao, J., Peng, Y., Xu, Z., Chen, R. Q., Gu, Q. H., Chen, Z., Lu, W. (2008) Synaptic metaplasticity through NMDA receptor lateral diffusion. J Neurosci, 28, 3060–3070.

FIGURE 1

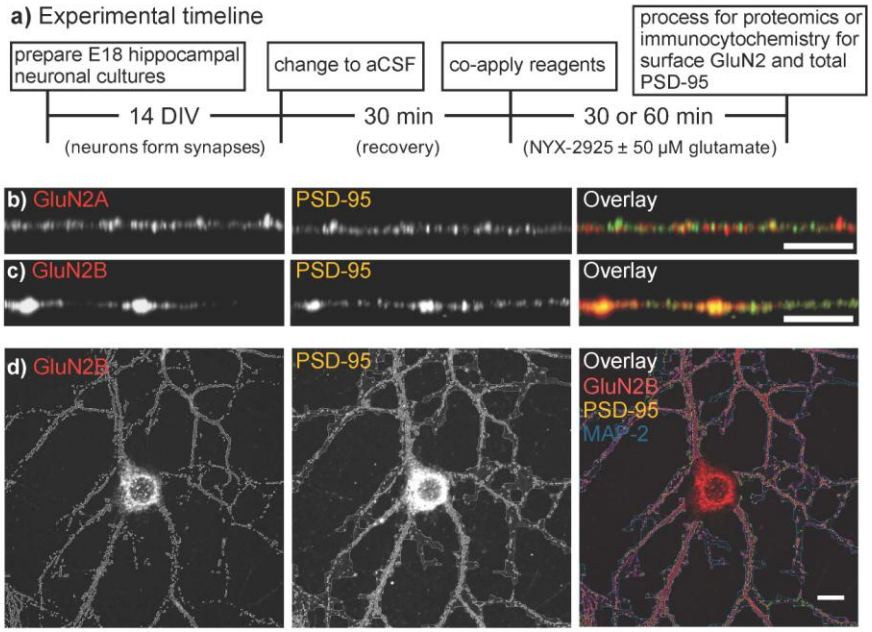

Bowers, M.S. et al.

FIGURE 2

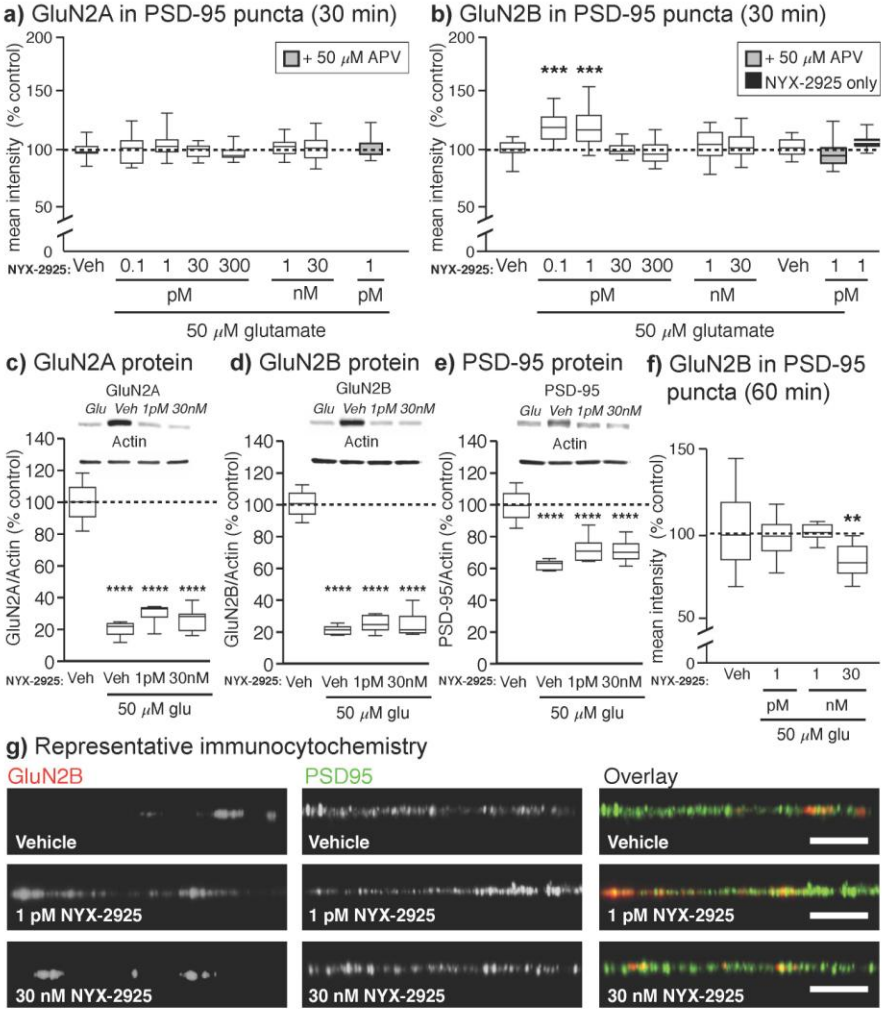

Bowers, M.S. et al.

FIGURE 3

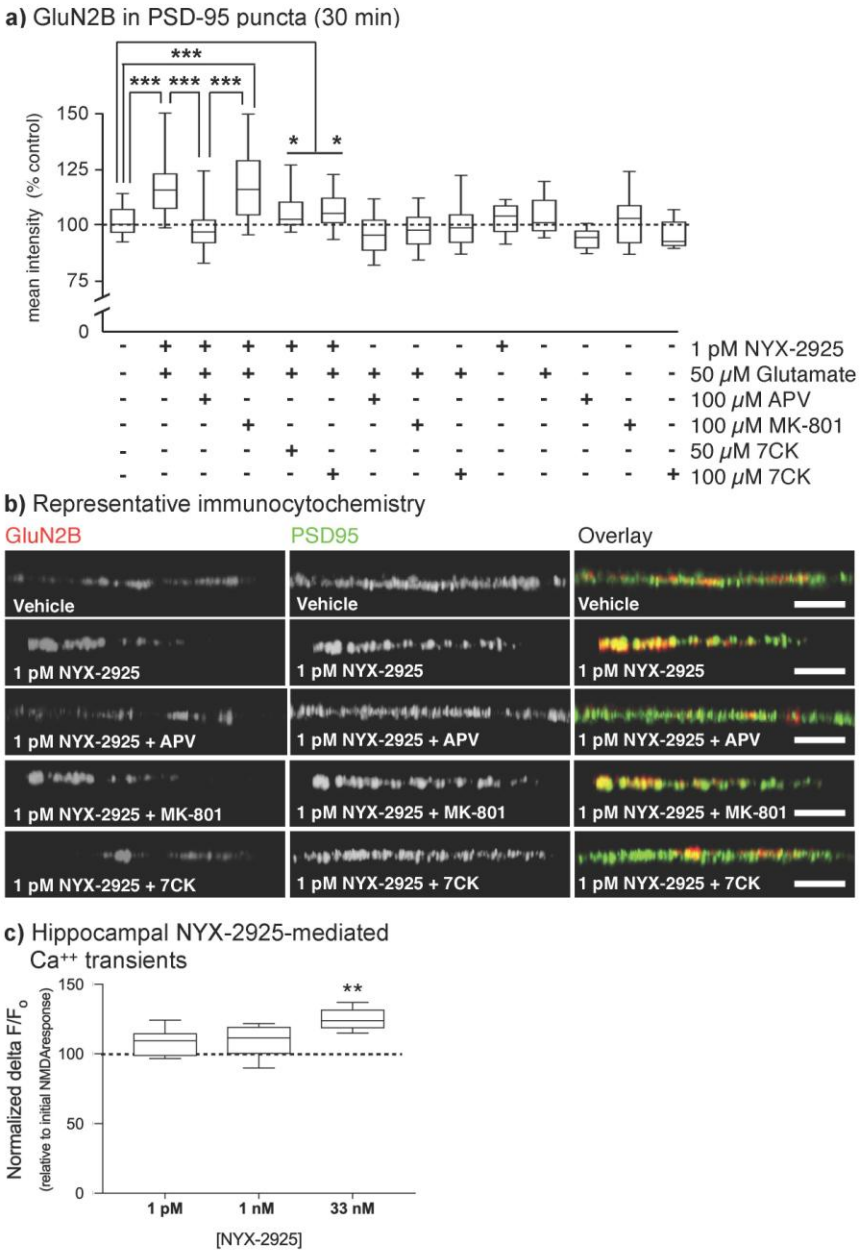

Bowers, M.S. et al.

FIGURE 4

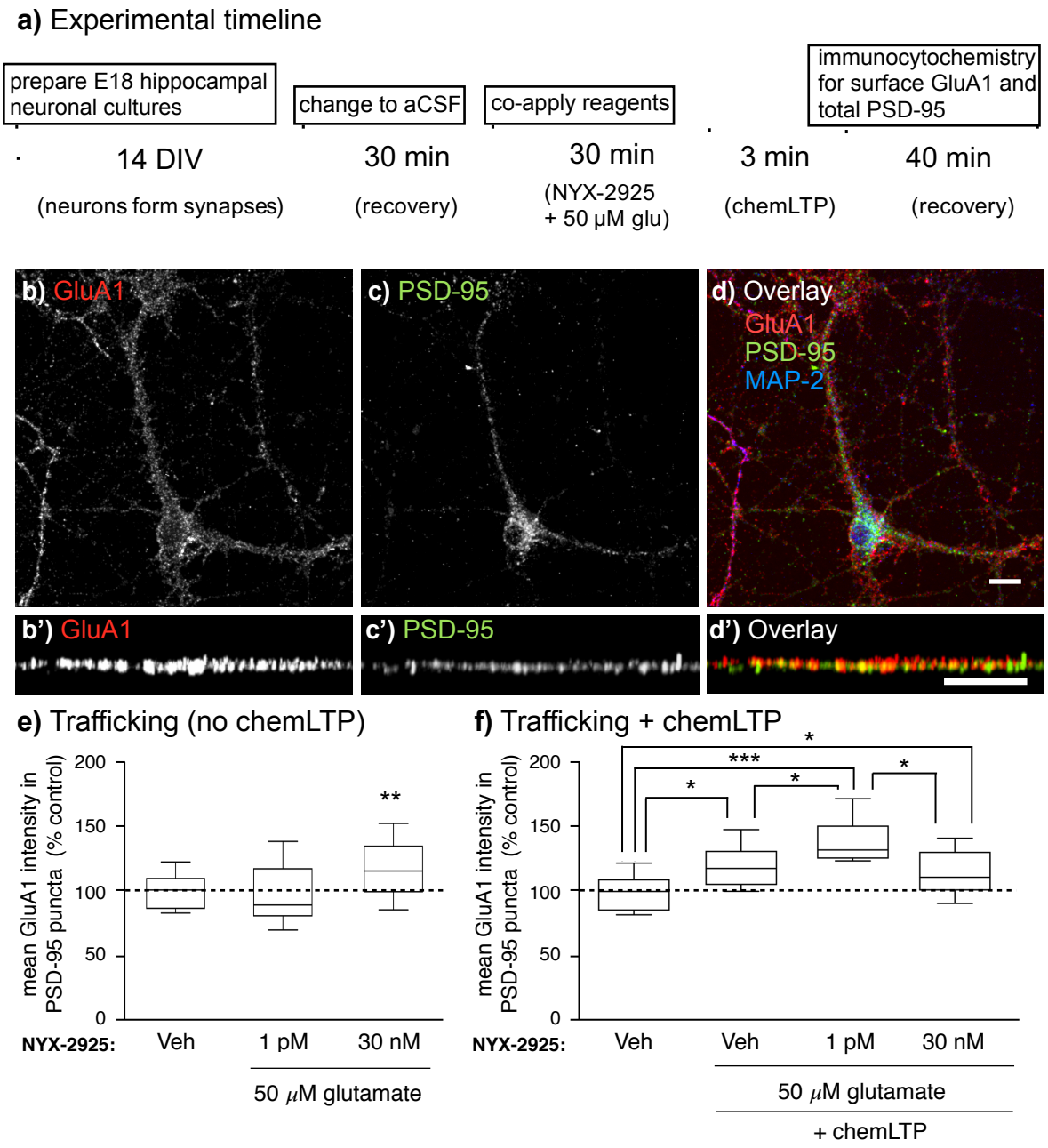

FIGURE 5

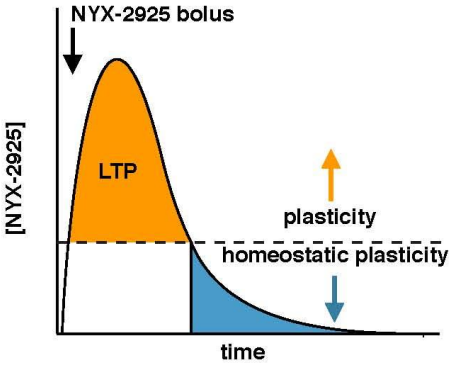

Bowers, M.S. et al.